Accepted Manuscript

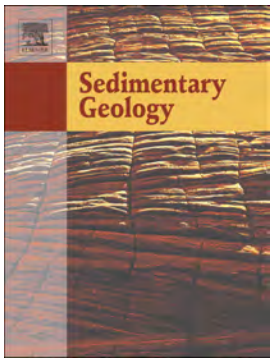

Glaciolacustrine deposits formed in an ice-dammed tributary valley in the south-central Pyrenees: New evidence for late Pleistocene climate

Carlos Sancho, Concha Arenas, Gonzalo Pardo, José Luis Peña-Monné, Edward J. Rhodes, Miguel Bartolomé, José M. García-Ruiz, Carlos Martí-Bono

PII: S0037-0738(18)30017-4
DOI: https://doi.org/10.1016/j.sedgeo.2018.01.008
Reference: SEDGEO 5306

To appear in:

Received date: 5 December 2017
Revised date: 30 January 2018
Accepted date: 31 January 2018

Please cite this article as: Carlos Sancho, Concha Arenas, Gonzalo Pardo, José Luis Peña-Monné, Edward J. Rhodes, Miguel Bartolomé, José M. García-Ruiz, Carlos Martí-Bono , Glaciolacustrine deposits formed in an ice-dammed tributary valley in the south-central Pyrenees: New evidence for late Pleistocene climate. The address for the corresponding author was captured as affiliation for all authors. Please check if appropriate. Sedgeo(2018), https://doi.org/10.1016/j.sedgeo.2018.01.008

This is a PDF file of an unedited manuscript that has been accepted for publication. As a service to our customers we are providing this early version of the manuscript. The manuscript will undergo copyediting, typesetting, and review of the resulting proof before it is published in its final form. Please note that during the production process errors may be discovered which could affect the content, and all legal disclaimers that apply to the journal pertain.

ACCEPTED MANUSCRIPT

Glaciolacustrine deposits formed in an ice-dammed tributary valley in the south-central Pyrenees: new evidence for late Pleistocene climate

Carlos Sancho[1], Concha Arenas[1*], Gonzalo Pardo[1], José Luis Peña-Monné[2], Edward J. Rhodes[3], Miguel Bartolomé[4], José M. García-Ruiz[4], Carlos Martí-Bono[4]

[1] Departamento de Ciencias de la Tierra, Universidad de Zaragoza, Pedro Cerbuna 12, 50009 Zaragoza, Spain

[2] Departamento de Geografía y Ordenación del Territorio, Universidad de Zaragoza, Pedro Cerbuna 12, 50009 Zaragoza, Spain

[3] Department of Geography, The University of Sheffield, Sheffield S10 2TN, UK

[4] Instituto Pirenaico de Ecología, Consejo Superior de Investigaciones Científicas (IPE-CSIC), Apartado 13.034, 50080 Zaragoza, Spain

* Corresponding author

ACCEPTED MANUSCRIPT

Abstract

Combined geomorphic features, stratigraphic characteristics and sedimentologic interpretation, coupled with optically stimulated luminescence (OSL) dates, of a glacio-fluvio-lacustrine sequence (Linás de Broto, northern Spain) provide new information to understand the palaeoenvironmental significance of dynamics of glacier systems in the

ACCEPTED MANUSCRIPT

south-central Pyrenees during the Last Glacial Cycle (≈ 130 ka to 14 ka). The Linás de Broto depositional system consisted of a proglacial lake fed primarily by meltwater streams emanating from the small Sorrosal glacier and dammed by a lateral moraine of the Ara trunk glacier. The resulting glacio-fluvio-lacustrine sequence, around 55 m thick, is divided into five lithological units consisting of braided fluvial (gravel deposits), lake margin (gravel and sand deltaic deposits) and distal lake (silt and clay laminites) facies associations. Evolution of the depositional environment reflects three phases of progradation of a high-energy braided fluvial system separated by two phases of rapid expansion of the lake. Fluvial progradation occurred during short periods of ice melting. Lake expansion concurred with ice-dam growth of the trunk glacier. The first lake expansion occurred over a time range between 55±9 ka and 49±11 ka, and is consistent with the age of the Viu lateral moraine (49±8 ka), which marks the maximum areal extent of the Ara glacier during the Last Glacial Cycle. These dates confirm that the maximum areal extent of the glacier occurred during Marine Isotope Stages 4 and 3 in the south-central Pyrenees, thus before the Last Glacial Maximum. The evolution of the Linás de Broto depositional system during this maximum glacier extent was modulated by climate oscillations in the northern Iberian Peninsula, probably related to latitudinal shifts of the atmospheric circulation in the southern North-Atlantic Ocean, and variations in summer insolation intensity.

Key words: glaciolacustrine sediments; ice-dammed lake; maximum glacier extent; Marine Isotope Stages 4 and 3; south-central Pyrenees.

ACCEPTED MANUSCRIPT

1. Introduction

The south Pyrenean Quaternary glaciations have been the subject of study since the 19th century (see compilation by Chueca et al., 1998). Regional mapping and detailed geomorphology (Vilaplana, 1983; Bordonau, 1992; Martí-Bono, 1996; Serrano, 1998), and indirect dates from lacustrine records allowed refining the reconstruction of the glacial evolution (Montserrat-Martí, 1992; García-Ruiz et al., 2003; González-Sampériz et al., 2006). The asynchronous character of the maximum glacier advances in the south-central Pyrenees during the Last Glacial Cycle (LGC) relative to the Last Glacial Maximum (LGM) was then postulated. The LGC is defined as the last cold stage between Termination II (130 ka) and Termination I (14 ka) (Gibbard and Cohen, 2008; Hughes et al., 2013). Dating of glacial records based on optically stimulated luminescence (OSL) (Sancho et al., 2003; Lewis et al., 2009; García-Ruiz et al., 2013) and terrestrial cosmogenic nuclides (TCN) (Delmas et al., 2008; Pallás et al., 2010; Calvet et al., 2011) confirmed such a hypothesis. Dating the maximum ice extent through the Mediterranean realm during the LGC (e.g., Hughes et al., 2006a, b, 2013; Hughes and Woodward, 2008) is a matter of debate during the last decade in other mountains in the Iberian Peninsula (e.g., Palacios et al., 2011; Jiménez-Sánchez et al., 2013; Dominguez-Villar et al., 2013; Carrasco et al., 2015; Rodríguez-Rodríguez et al., 2016).

Glaciolacustrine environments are exceptionally sensitive to environmental changes and climate oscillations at different time scales (e.g., Matthews et al., 2000; Gruszka, 2001; Johnsen and Brennand, 2006; Shulmeister et al., 2010; Turu et al., 2017; Smith, 2017). The southern Pyrenean glacial records include glaciolacustrine deposits, e.g., in

ACCEPTED MANUSCRIPT

the River Aragón Subordán valley (La Reclusa) (Martí-Bono, 1977), the River Gállego valley (Aso de Sobremonte) (Serrano, 1998), the River Esera valley (Cerler) (Bordonau, 1992), the River Noguera Ribagorzana valley (Llauset and Llestui) (Serrat et al., 1982; Vilaplana et al., 1983, 1989; Monserrat and Vilaplana, 1988; Bordonau et al., 1993) and the River Valira valley (La Massana) (Serrat et al., 1982; Turu, 2002; Turu et al., 2017). Among these, the glaciolacustrine sequence of Linás de Broto, formed in relation to ice-damming by the River Ara valley (Huesca Province), constitutes a classical record in the south-central Pyrenees, known since the late 19th century (Mallada, 1878; Penck, 1883; Serrat et al., 1982; Martí-Bono and García-Ruiz, 1994; Martí-Bono, 1996; Martí-Bono et al., 2002).

Although previous work on the glacio-fluvio-lacustrine record of Linás de Broto has dealt with geomorphology (Martí-Bono, 1996), sedimentology (Serrat et al., 1982) and chronology (Martí-Bono et al., 2002; Sancho et al., 2011), conclusive results in regard to timing and depositional evolution of such record in relation to climatic parameters and other glacial records are still missing. As a consequence, this work aims to i) define precisely the depositional evolution of this glacio-fluvio-lacustrine sequence with respect to the relevant sedimentary processes and climatic conditions, and ii) place this record chronologically within the evolution of the south Pyrenean glaciation during the LGC. For this purpose, new geomorphologic, sedimentologic and chronologic (based on OSL) data of the Linás de Broto sequence have been obtained.

2. Study area

ACCEPTED MANUSCRIPT

In the south-central Pyrenees (northern Spain) (Fig. 1A), the Quaternary glaciofluvial and glaciolacustrine deposits of Linás de Broto, which are the focus of this work, fill the lower reach of the River Sorrosal valley, a tributary of the River Ara valley (Fig. 2A).

From a geological point of view (Fig. 1B), the study area is located in the south Pyrenean thrust-and-fold belt (Muñoz, 2002). The outcropping bedrock in the River Sorrosal watershed is composed of Upper Cretaceous-Paleocene limestones, dolostones and sandstones of the Internal Sierras, and Eocene turbidites of the Jaca Basin (Barnolas and Pujalte, 2004) (Fig. 2A). These materials show a complex structure with tight folds and imbricated thrust sheets (Ríos et al., 1982).

Present climate in the Sorrosal valley bottom is cool temperate (Oceanic-Mediterranean transition), with a mean annual temperature of 8.5-9.0 °C and a mean annual precipitation of around 850 mm (López et al., 2007). However, colder conditions (around 0°C of average annual temperature, following estimations from Del Barrio et al., 1990) with high snowfall (more than 2000 mm of annual precipitation, as deduced from De la Riva, 2000) dominate the highest areas of the watershed (up to 2845 m).

The present landscape of the River Sorrosal watershed, with an area of 42 km^2, is related to fluvial incision and glacial activity persisting throughout the Quaternary on the deformed Mesozoic-Cenozoic bedrock. Pleistocene deposition is represented by moraines, glaciolacustrine deposits and staircase fluvial terraces (Martí-Bono, 1996) (Fig. 2A). A sharp escarpment related to three small coalescent glacial cirques, formed within folded Upper Cretaceous-Paleocene rocks, occurs in the northern sector of the

ACCEPTED MANUSCRIPT

River Sorrosal watershed. The upper sector of the valley presents U-shaped morphology, and moraine remnants corresponding to three stages of glacier stabilization can be recognized (S1, S2 and S3 in Fig. 2A). Slope and periglacial morphologies (rock glaciers) complete the landscape of the uppermost sector of the River Sorrosal valley (Fig. 2A).

A moraine formed of two very close ridges, separated by a paleovalley, can be distinguished near the village of Viu (A1.a and A1.b in Fig. 2B). It was deposited as a lateral moraine during the maximum extent of the Ara glacier, an ice tongue around 32 km in length flowing from the Vignemale massif (3299 m a.s.l.), when it was approximately 400 m thick at that sector and terminated near the Asín de Broto village (800 m a.s.l.), approximately 8.5 km down-valley from the Viu morraine (Serrano and Martínez de Pisón, 1994; Martí Bono et al., 2002) (Fig. 2C). A sedimentary unit made of gravels and sands, probably related to a kame terrace deposited against till deposits, has been recognized on the southwestern side of the Viu moraine (Martí-Bono, 1996) (A1.c in Fig. 2B). Sand lenses in this kame terrace deposits were sampled for OSL dating (Sancho et al., 2011).

At present, the morphogenetic surface associated with the fluviolacustrine deposits (Q1 terrace in Fig. 2A, B) is 60 m above the present river channel. The deposits of terrace Q1 comprise fluvial and lacustrine facies. The geomorphic relationship between the external lateral moraine of the Ara glacier (i.e., Viu moraine; A1 in Fig. 2B) and the glaciolacustrine record to the west-northwest (e.g., locus of measured sections LB1 and LB2, Fig. 2B) in the Pleistocene is very clear, taking into account the relative spatial position and elevation of the top of the glaciolacustrine deposits and the

ACCEPTED MANUSCRIPT

external moraine. Upstream of Linás de Broto (north of the village), the Q1 terrace of the River Sorrosal has been identified forming an elongated (2.7 km) and very narrow bench on the east side of the valley (Fig. 2A).

Another lateral moraine of the Ara glacier is located close to the village of Fragen (A2 in Fig. 2B); its more internal position respect to the Viu moraine (A1 in Fig. 2B) indicates a later retreat stage of the glacier. The occurrence of a small lake related to that lateral moraine in Fragen is not rejected, but any related lacustrine deposits have not been recognised in the field. This younger aggradational glacier stage may explain the middle staircase terrace identified along the River Sorrosal at Linás de Broto and other upstream sites on the right side of the valley (Q2 terrace in Fig. 2A, B). Finally, a lower staircase terrace related to the River Sorrosal has been identified around the village of Linás de Broto (Q3 terrace in Fig. 2A, B).

In brief, in Pleistocene times at least two stages (Viu and Fragen glacial phases) of the Ara glacier stabilization can be deduced from preserved lateral moraines at Viu and Fragen (A1 and A2 in Fig. 2A, B). The Viu phase represents the maximum ice advance of the Ara glacier during the LGC (Serrano and Martínez de Pisón, 1994; Martí-Bono, 1996). The Sorrosal glacier did not join the Ara glacier, and a proglacial lake separated these two glaciers. The deposits of such a lake (represented in terrace Q1) are studied in this paper.

3. Methods

An aerial photographic base (Interministerial flight 1978, scale 1:18,000; Aragón flight 2006, scale 1:30,000) and Google Earth images from 2016 were used for mapping of

ACCEPTED MANUSCRIPT

the River Sorrosal catchment. Extensive field investigations and mapping were undertaken to confirm the presence and nature of mapped moraines, lacustrine deposits and terraces. At a natural scarp formed by the incision of the River Sorrosal close to the villages of Linás de Broto and Viu, two stratigraphic-sedimentologic sections were measured through the Quaternary deposits (LB1 and LB2; Figs. 2B, 3). The outcrops were logged and correlations between the stratigraphic sections made using a composite panoramic photographic image (Figs. 3, 4A). Sedimentary facies were characterized on the basis of lithology, bed geometry, texture and sedimentary structures. The sedimentary lithofacies codes of Miall (1978) were used in sedimentologic analysis (Table 1), and lithofacies associations were established. Laminated facies were studied for textural and structural characterization with thin sections (from eight samples) using a petrographic microscope. Scanning electron microscopy (SEM) was applied to help mineral identification using X-ray elemental microanalyses (Carl Zeiss MERLIN™, Carl Zeiss Group, Jena, Germany) in the case of four fine-grained samples, operating at 3-5 kV and 150-500 pA. Powder from four fine-grained samples was used to establish the mineralogical composition by X-Ray Diffraction, using a D-Max Rigaku diffractometer equipped with a graphite monochromator and CuKa radiation. XRD and SEM determinations were made at the *Servicios de Apoyo a la Investigación* (SAI) of the University of Zaragoza (Spain).

Optically stimulated luminescence (OSL) dating was undertaken using well-sorted sandy deposits from section LB1 (Fig. 3), and preliminary results were first presented by Sancho et al. (2011), although methods were not explained or the implications discussed in that summary. The OSL analyses of four samples (Table 2) were performed

ACCEPTED MANUSCRIPT

at the Luminescence Dating Laboratory of the Research Laboratory for Archaeology and the History of Art (University of Oxford, UK). Quartz grains within the size range of 125-250 μm were extracted as described by Rhodes (1988). Sample preparation included sieving, etching with concentrated hydrofluoric acid (HF), and sodium polytungstate density separation of heavy minerals. A single aliquot regenerative-dose (SAR) protocol (Murray and Wintle, 2000, 2003) was used for OSL dating, with measurements made on a Risø TL-DA-15 automated luminescence reader. In-situ gamma ray spectrometry (Rhodes and Schwenninger, 2007) was used to estimate the environmental dose rate. Using values derived from measured water content samples, a value of 15±5% was applied in the age calculations.

4. Stratigraphy and sedimentology

4.1 Stratigraphic sections

Two stratigraphic sections were measured to the southeast of Linás de Broto (location in Fig. 2B). These sections –LB1 and LB2– are 56 and 53 m thick, respectively (Fig. 3). The lowest part of the outcropping succession can be observed on a scarp excavated by lateral erosion of the present River Sorrosal between these sections. That part consists of ≈ 2.5 m thick alternating gravel and sand beds (Figs. 3, 4B).

In these sections eighteen sedimentary facies were identified based on lithology, bed geometry, texture and sedimentary structures. Their main textural and structural features, and their depositional interpretation are summarized in Table 1 and are illustrated in Figures 4 to 9.

ACCEPTED MANUSCRIPT

Gravels are present along the two sections (Fig. 3). Many parts of them are structureless (facies Gm), occasionally with clast imbrication, though horizontal stratification and trough and planar cross-stratification (facies Gh, Gt and Gp) are present (Fig. 5A-F).

Sands form centimetre- to decimetre-thick, tabular and less common lenticular bodies that can be structureless (Sm), but commonly show horizontal lamination (Sh), ripple lamination and ripples (Sr) (Fig. 6). Flame structures and contorted lamination are conspicuous features of these facies (Fig. 9). Lense- and sigmoid-shaped coarse-sand bodies, decimetre-thick, form foreset cross-stratification (Sf). In some cases, facies Sf associate laterally and vertically to facies Gf and Gm, e.g., at the base of the studied sequence (Figs. 4B, 5F-H).

Silts and clays are more abundant in section LB2, being either structureless (Fm and Clm) or with horizontal and ripple lamination (Fh, Clh and Fr) (Figs. 7, 8). Dropstones (mm to ≈ 1 m long) are common in the clay layers. In some areas, beds formed of sands and silts, and minor gravels, show metre-scale folds (Fig. 9A, B).

Five lithological units were differentiated and correlated based on the physical continuity of several gravel bodies throughout the outcropping deposit (Figs. 3, 4A).

Unit 1 is 12 m thick in LB1 and 8.3 m thick in LB2. It is mostly formed of clast-supported gravels with minor sands and occasional mud intercalations. With respect to grain size, maximum values varies between 19 and 32 cm in LB1 and between 15 and 22 cm in LB2. Single larger clasts, 0.5 to 1.2 m long, appear in the upper third of the unit. These coarse facies form tabular bodies, up to 3 m thick, with irregular and erosive bases,

ACCEPTED MANUSCRIPT

and may show gentle concave internal surfaces. Most common facies in Unit 1 are Gm and Gh, along with Gt and Gp that are associated with St and Sp (see Table 1 for facies codes). Fining upward deposits, up to 0.6 m thick, made of Gh and Sh are more common in section LB2. Sands may also constitute lenticular bodies, cm to 0.2 m thick, either as Sm, Sh or St. Lenticular bodies of muds (mainly silts), up to 0.2 m thick, are interbedded within facies Gm and Gh.

Unit 2 is approximately 22 m thick in both sections. This is an heterolithic interval with a clear predominance of sandy facies. Gravels are minor in LB2, while silts and clays become more abundant than in LB1. Sands form tabular strata, cm to dm thick, and display a wide array of facies (Sm, Sr1, Sr2, Sh, St and Ss); in-phase and in-drift climbing ripple lamination (type C of Jopling and Walker, 1968; or type 1 of Reineck and Singh, 1980; or type B of Ashley, 2002) is a noticeable feature. Gravels, with clasts up to 10 cm long, constitute wedge-shaped bodies up to 0.5 m thick in section LB1 that become thinner or pass laterally into finer facies in section LB2; most common facies are Gm, Gh, Gt and Gf. In all cases, sand- and gravel-size deposits wedge out southeastward (from LB1 to LB2), as the thickness of finer-size deposits increases, which indicates the transport direction of sediment. Well-sorted sands from three levels in Unit 2 were samples for OSL dating. Silts and clays form tabular or wedge-shaped intervals up to 3 m thick and show a great variety of facies, both structureless and with ripple and horizontal lamination. Fine, rhythmic lamination (Clh) is more noticeable towards the upper part of this unit, in particular in section LB2, where laminated intervals can be up to 5 m thick. In many cases, deformation structures (e.g., flames, contorted laminae

ACCEPTED MANUSCRIPT

and micro-grabens) are present. Dropstones, mm to cm long, are common within silt and clay facies (Fig. 7B, F).

Unit 3 consists of a slightly wedged, massive body, up to 6.5 m thick in section LB1, mostly formed of structureless gravels (facies Gm, and minor Gh) with occasional, 0.3 m thick, lenticular bodies of sands (St, Sh). Clasts are up to 25-28 cm long in LB1 and decrease to 20-23 cm in LB2.

Unit 4 is about 5 m thick in LB1 and 10.5 m thick in LB2. In LB1, it is formed of tabular gravel bodies (facies Gm and Gh, with clasts up to 20 cm long) that alternate with laminated clay intervals (Clh, up to 1.1 m thick) that contain dropstones up to 43 cm long. In LB2, thin gravel (dm thick; clast size < 10 cm) and minor sand beds are interbedded within thicker (up to 4 m minimum, at the base of Unit 4) clay intervals, making a coarsening upward sequence.

Unit 5 is about 10 m thick in LB1 and 5 m thick in LB2. It is mostly made of massive gravels (facies Gm and minor Gh), with clasts up to 20-25 cm in LB1 and 40 cm in LB2, and occasional, decimetre-thick, lenticular sand beds (facies Sm and Sh) at the base.

4.2 Facies associations

Lateral and vertical relationships between the sedimentary facies can be expressed by up to twelve facies associations (FA), i.e., simple vertical sequences (Fig. 10), that correspond to three main depositional environments/settings: i) fluvial (braided river), ii) lake margin (deltaic foresets and prodelta and subaqueous mass flows), and iii) distal lake area or lake bottom plain (offshore areas). The main facies and facies associations along the stratigraphic sections are indicated in Figure 3.

ACCEPTED MANUSCRIPT

4.2.1 Fluvial facies associations (FA 1A and 1B, Fig. 10).

a) FA 1A [Gm -> (Gp—Sp), (Gt—St) -> Gh <-> (Sm, Sh) -> Fm]. This fining-upward FA represents deposits of a braided streams with longitudinal and transverse bars (Gh, Gp and Sp), shallow channels that can be filled with sinuous-crested dunes (Gt and St; Miall, 1977; Allen, 1982a, b), and sand sheet deposits (Sm and Sh). Massive fines (Fm) are very rare and form very thin deposits, representing waning of currents. Their scarcity probably was due to the small size of the floodplain and/or common erosional processes over this narrow valley area (cf., Arenas et al., 1989). These features along with the textural attributes (e.g., poor sorting and low roundness) suggest that the sequence represents sedimentation in a high energy braided fluvial system close to the sediment source area (i.e., equivalent to proximal to middle "outwash plain"). Unit 1 in the two sections LB1 and LB2 is formed of several fining-upward sequences that correspond to either the complete or incomplete FA 1A (Fig. 5A, B).

b) FA 1B [Gh, Sh -> (St), (Sm) -> Gm]. This coarsening-upward FA represents progradation of the fluvial system, with gravel beds (Gm, from flash floods) over small sand or gravel bedforms (Sh, Sm or Gh, from longitudinal and crescent bars), mostly developed under subaerial conditions. FA 1B is recognized in Units 3 and 5.

4.2.2 Lake margin associations: coarsening upward (deltaic and subaqueous mass flows) and fining upward (turbidite-like deposits) facies associations.

a) *Coarsening upward associations* (FA 2A, 2B and 3A, Fig. 10).

FA 2A [(Fh, Sh) -> Sr1, Sr2, (Sm) -> Gf—Sf] consists of gravel and sand foreset stratification overlying rippled and laminated sands and silts. It represents deposition

ACCEPTED MANUSCRIPT

of small gravel and coarse sand bars that prograded on the lake margin, forming foresets (Gf and Sf) that suggest that sediments delivered to the delta avalanched and rolled down the delta front (Johnsen and Brennand, 2006; Winsemann et al., 2007). This FA is well developed at the base of the studied succession (between sections LB1 and LB2; Figs. 3, 4B, 5F to 5H) and in Unit 2 (Fig. 6F).

FA 2B [Clm <-> Fh, Clh <-> Sr1, Sr2, Fm] corresponds to prodelta deposition, relating to fine sandy and silty sediment that flowed down the delta front as hyperpycnal flow (e.g., Kostic et al., 2005; Johnsen and Brennand, 2006). Climbing ripples in FA 2 (Fig. 6B) provide evidence of rapid deposition from sediment-laden unidirectional flows in a standing body of water (Jopling and Walker, 1968; Allen, 1970, 1971; Stanley, 1974; Pietras and Carrol, 2006). The general coarsening upward evolution is due to delta progradation during increased sediment inputs. This FA is present in Unit 2 at section LB1.

FA 3A [Fm, Fh, Fr -> Gh, Sh -> Gm] was formed by suspension setting and low energy traction currents (Fm, Fh, Fr), followed by rapid deposition from high-velocity expanding jets that carried medium to coarse sediment (Gm, Gh, St, Sh, Sm) onto the lake margin. The coarser deposits (Gm) may correspond to debris-flow deposits (e.g., Winsemann et al., 2007; Evans et al., 2013) and other unconfined gravity flows (e.g., as described by Ashley, 2002). This FA is present in Unit 2 in section LB1 (Figs. 3, 7A).

b) *Fining-upward associations* (FA 4A, Fig. 10).

FA 4A [Gm, (Gh) <-> Clm -> Clh] resulted from deposition of sediment from meltwater streams that entered the lake as density currents forming coarse sediment drapes or

ACCEPTED MANUSCRIPT

lobes (Gm and Gh), and fine sediment deposits from suspension settling (Clm and Clh) in a relatively deep water body, as evidenced by dropstones in the clay facies. This FA represents deposition from dense turbidity currents (Gruszka, 2007; Eyles and Eyles, 2010) in middle to distal lake areas. This FA is recognized in Unit 4 (LB1 and LB2) (Figs. 3, 7B).

4.2.3 Distal lake associations.

a) *Coarsening-upward associations* (FA 2C, 3B and 5, Fig. 10).

FA 2C [Fr, Sh -> Ss -> Sr2, St—(Gt)] (Fig. 6E) and 3B [Fh <-> Clh -> Sm, Sh <-> Gm] represent lacustrine deposition from highly energetic flows that reached distal deltaic areas that had previously been sites for fine deposition (facies Fr, Fh, Clh). These underflows gave rise to silty and sandy bedforms (Sr2 and St), including scour and fill structures (i.e., Ss in sequence 2C). In addition, sheet-like density flows that carried sand and fine gravel formed tabular beds (Sm, Sh and Gm) located at the top of sequence 3B.

FA 5 [Clm -> (Clh) -> Fm -> Sm] represents deposition in a more distal area and/or corresponds to lower-competence flows, compared to FA 2C and 3B. Facies Clm, Fh and Clh at the base of the three FA indicate fine sediment deposition from suspension by settling. Thick and extensive fine deposits formed during periods of high water level in the lake, when the lake was larger.

b) *Fining-upward and rhythmic associations* (FA 4B, 6A and 6B, Fig. 10).

ACCEPTED MANUSCRIPT

These FA are characterized by having dominant fine sediments that show thin lamination or are structureless (Fig. 7C-F). These fine sediments (facies Fm, Clm and Clh) formed mainly by settling from suspension in offshore areas. Lamination in these fine grained deposits is formed of rhythmites (Fig. 8A, B), which consist of alternating thin silt laminae (submillimetre-thick) and thicker clay laminae (submillimetre- to millimetre-thick), or solely clay laminae of different colours. Some laminae show gradual fining-upward evolution from silt to clay, but commonly the two grain-size intervals are clearly separated (Fig. 8C). Sand-size grains in facies Clh correspond to angular dropstones (Fig. 8D). These rhythmites suggest the absence of significant coarse or middle-size sediment input that reached the lake centre, thus with coarse sedimentation likely limited to the lake margins. Probably, each rhythmite pair corresponds to a pulse of meltwater input, as proposed for some lake deposits (Desloges, 1994), but it can also result from deposition by distal turbidity currents without seasonal control (Ashley, 2002). In turn, the deposits of facies Sm, Sh, Sr and Fr in FA 4B and 6A indicate that current dynamics reached the distal lake areas, likely as density currents (e.g., as reported by Krzyszkowski, 1994; Gruszka, 2007). Thus, these sequences would reflect the succession or alternation of hyperpycnal flow turbidites (producing sandy deposits) and the tail of turbidity currents or quiet-water deposition from suspension (producing laminated silts and clays), as reported by Johnsen and Brennand (2006). In addition, ice-rafted dropstones, submillimetre to rare centimetre long, though not abundant, caused soft deformation of the laminae (Fig. 8D; e.g., as described by García et al., 2015). Rhythmic laminated silts and clays are common in many Pleistocene glacial lakes (e.g., Gruszka, 2007; Evans et al., 2013; Smith, 2017).

ACCEPTED MANUSCRIPT

Deformation structures are present in almost all facies types. These structures include intraformational folds (cm to m high) in gravel and sand deposits (Fig. 9A, B), convoluted lamination/bedding in sandy to muddy deposits and sand and silt flames (Fig. 9D-F), and rare micro-faulting in sandy and muddy deposits (Fig. 9C), which together denote deformation driven by depositional, climate (controlled by melting-freezing processes of porewater) and/or tectonic (seismic) factors (Gruszka, 2001; Smith, 2017). Evidence for seismic origin is not always clear and many deformation structures might have been related to climatic and depositional processes. Soft sediment deformation structures in silt-rich sediment can be caused by overpressuring of porewater during freezing (Eyles and Eyles, 2010; Smith, 2017), and also can form during fluid escaping from sediments that have been deposited rapidly (Cheel and Rust, 1986; Prior and Bornhold, 1988; Johnsen and Brennand, 2006; Evans et al., 2013). The asymmetric deformation shapes of ripples, ripple lamination and sand and silt convolution in the study area suggests a flow component that is parallel to sediment transport direction, and thus indicates the effects of traction currents over soft sediment deposited at high rates (Fig. 9D).

4.3 Depositional environment evolution

Geomorphologic, stratigraphic and sedimentologic information allows us to reconstruct depositional evolution of the glaciofluvial and glaciolacustrine systems of Linás de Broto through time (Fig. 11). The ice tongue of the Ara trunk glacier dammed a braided gravelly fluvial system that was fed by meltwater from a small glacier that was present in the headwater of the River Sorrosal tributary valley. As a result, an extensive proglacial fluvial and lacustrine depositional system was developed near

ACCEPTED MANUSCRIPT

Linás de Broto (Figs. 2A, 11, 12). The system was also fed by slope runoff and sediment derived from the whole watershed. Only minor inputs from the Ara glacier (through icebergs and meltwater transporting particles from the Viu moraine) are inferred from the lithological nature (granite) of some clasts in gravels. The lake was approximately 0.5 km wide and 1.5 km long (minimum dimensions, based on extent of present outcrops).

Unit 1 is referred to as FA 1A (Fig. 10) and represents deposition in shallow bars and channels of a braided fluvial system (outwash train) with dominant subaqueous traction of high competence and capacity. Similar deposits have been reported from proximal and proximal-middle sectors of glaciofluvial systems (Evans et al., 2013; García et al., 2015). The presence of vertical clasts indicates dispersive pressure after deposition in high energy conditions (Allen, 1981). Erratics (single clast up to 1.2 m long, Fig. 5E) support the association of these deposits within a glacial setting, as these clasts only could be transported as sediment within floating- or rafting-ice masses carried by the fluvial currents. The fluvial system also formed small coarse gravel deltaic lobes (FA 2A, Fig. 10) that extended eastward and southeastward into the lake (i.e., deposits that crop out below Unit 1, between sections LB1 and LB2; Figs. 3, 4B, 5F), as indicated by facies distribution through space and bedform palaeocurrents.

The general vertical sedimentary evolution of Unit 1 is fining upward. The clast size decreases and the amount of sand-size facies increases from LB1 to LB2. Together, the vertical and lateral evolution can be interpreted as a retrogradation stage of the fluvial system following peak deposition that occurred in high energy conditions.

ACCEPTED MANUSCRIPT

In Unit 2, FA are varied and correspond to both marginal (FA 2A, 2B, 3A and 3B) and distal lake deposits (FA 2C, 4B, 5, 6A and 6B) (Fig. 10). As a whole, the deposition of Unit 2 is mostly related to coarse sedimentation on the lacustrine margin (i.e., as small deltaic lobes, FA 2A, and gravity deposits from unconfined flows, FA 3A and 3B) and finer sedimentation towards more internal lacustrine zones (i.e., to more dilute bottom flows and settling out). Fine sand and silt facies intercalated within laminated clay sediments formed by settling out in offshore lacustrine zones (Fig. 11A, stage 2). These facies and the associated processes have been recognised in some ice-contact lakes (Ashley, 2002) that receive coarse detrital inputs.

The sharp contact between Units 1 and 2 (with respect to lithology, with Unit 2 beginning with fines over gravels of Unit 1) represents rapid lake expansion. The general vertical sedimentary evolution of Unit 2 is first coarsening-upward, then fining-upward. In the lower half, coarsening-upward sequences are dominant; the rest is composed of both fining- and coarsening-upward sequences, although coarsening-upward sequences dominate in LB1. As a whole, these features suggest progradation followed by retrogradation of the fluvio-deltaic system in the context of a general expansion of the lake, which is consistent with the increased thickness and abundance of fine sediment deposits (i.e., facies Clm, Clh and Fm) and decreased thickness and abundance of coarse facies toward the upper half of this unit.

Unit 3, mostly formed of massive gravels with occasional sands, is characterized by FA 1B. Deposition of this unit is related to a period of high discharge of the fluvial system. The vertically orientated clasts confirm dispersive processes and rapid deposition in high energy conditions (Allen, 1981), i.e., upward orientation of the clasts under the

ACCEPTED MANUSCRIPT

influence of high pressure through fluidized sediment. Together, deposition of Unit 3 represents the invasion of a large extent of the lake area with alluvial deposits. This drastic lake-area reduction or even disappearance could be concurrent with a lowering of the lake level (Fig. 11B, stage 3).

Unit 4 deposits, represented by FA 6B, 6A and 4A (Fig. 7B, D-F), formed following a very rapid lake expansion; on the lake margins, coarse sediments deposited from unconfined bottom flows could reach more internal zones. In these inner lacustrine zones, settling from suspension was the dominant process (e.g., as represented by stage 2 in Fig. 11A). Unit 4 shows a sharp basal contact with the underlying gravels.

Unit 5, formed of massive gravels (FA 1B), together with Unit 4, constitute a coarsening upward macrosequence resulting from progradation of the fluvial system that entered the lake. The massive character of this unit reflects dominant flash flood processes associated with intense meltwater currents that extended southeastward, and coincided with the final fill of the lake. Stage 3 in figure 11B would represent the beginning of such scenario.

In summary, the general evolution of the two sections reflects a complex expansion-retraction process of the lake that occurred in parallel with a complex retrogradation-progradation process of the high-energy braided fluvial system that entered the lake (Fig. 11). Section LB1 records deposition in more proximal zones, both in fluvial and marginal lacustrine settings, while section LB2 reflects more distal sedimentation of the fluvial system (e.g., as dense bottom flows) and primarily offshore lacustrine, in many cases rhythmic, sedimentation by settling during lake expansion stages.

ACCEPTED MANUSCRIPT

Final fill of the depositional area coincided with progradation of the fluvial system and lake opening by failure of the Ara glacier ice and moraine dam; subsequently, fluvial incision of the Viu moraine and of the Q1 deposits started.

5. OSL chronological data

Results from optically stimulated luminescence (OSL) dating of three samples from section LB1 (Fig. 3) and one sample from the terrace kame deposits that laterally overlie the Viu moraine (A1.c in Fig. 2B) are discussed here (Table 2). Samples X1600 (metre 21 of Unit 2) and X1598 (metre 33-34 of Unit 2) provided age estimates in the correct stratigraphic order: 55±9 ka, and 49±11 ka, for the middle and upper parts, respectively, of Unit 2 in section LB1 (Fig. 3). Sample X1599, between these two, provided an apparent age of 82±6 ka. Probably the age provided by sample X1599 is overestimated, given its stratigraphic position relative to the other dated samples, which provided age estimates consistent with each other. Sample X1601, from the terrace kame deposits, gave an age estimate of 49±8 ka, which is consistent with the top of Unit 2 in the Linás de Broto sequence (Table 2). Therefore, the Viu moraine started to form slightly before that age. These ages are older than the age obtained by Martí-Bono et al. (2002) (30.4±0.4 ka BP) for this lacustrine record using AMS radiocarbon dating on concentrated pollen samples in a position equivalent to Unit 2. However, the age obtained by Martí-Bono et al. (2002) should be taken with caution because of 1) the difficulty to use concentrated pollen for AMS radiocarbon dating, and 2) the age of the samples is close to the limit of application of this technique.

ACCEPTED MANUSCRIPT

The analysed samples provided low yields of quartz grains, and also display relatively low signal sensitivity, variable and occasionally high levels of Infra-Red Stimulated Luminescence (IRSL, associated with feldspar grains or micro-inclusions), with poor recycling and/or high levels of thermal transfer for several aliquots. These characteristics are not ideal for OSL dating, leading to some caution in the interpretation of the results. However, the apparent agreement between three of the four samples dated suggests that the quartz grains in this area can provide age estimates that in general are internally consistent and are considered broadly reliable. Low sensitivities of these glaciogenic samples are likely related to relatively brief transport of the constituent grains since excavation from bedrock. For some samples, a small number of aliquots showed significantly higher D_e values than others. These are interpreted as representing occasional grains which had been insufficiently zeroed during sedimentation (short transport in high-turbidity flow conditions and sometimes beneath ice-cover) and they have been omitted for age calculations. Similar findings are also observed in other glaciated regions, including the Himalayas (Rhodes and Pownall, 1994) and Greenland (Rhodes, 2000).

6. Discussion

Geomorphologic evidence supports the hypothesis that the lateral moraine preserved close to the Viu village (Fig. 2A) corresponds to the maximum extent of the Ara glacier during the LGC (García-Ruiz and Martí-Bono, 1994). At this point the ice tongue coming from the Vignemale massif terminated around the Asín de Broto village (Serrano and Martínez de Pisón, 1994) (Fig. 2C). These authors proposed, based on morphological features and regional studies, that this ice advance was prior to LGM (point 3 in Fig.

ACCEPTED MANUSCRIPT

1B). Other more internal lateral moraines (e.g., the Fragen moraine, Fig. 2A) in this sector of the River Ara valley represent a subsequent retreat stage of the glacier (García-Ruiz and Martí-Bono, 1994). The Ara trunk glacier dammed a glaciolacustrine depositional system related to the maximum ice extent during the Last Glacial Cycle. Despite uncertainty of the obtained datings, it can be proposed tentatively that the studied sedimentary sequence lasted from Marine Isotope Stage 4 (MIS4, prior to 55±9 ka BP) to the middle MIS3 (approximately 49±11 ka BP). Together, these results allow two main points to be discussed below: 1) The climatic and hydro-climatic conditions during this period inferred from the evolution of the depositional sedimentary system, and 2) The significance of the maximum ice surface extent of the Ara glacier during the LGC at a regional scale.

6.1. Evolution of the glacio-fluvio-lacustrine depositional system of Linás de Broto

The stratigraphic and sedimentologic characteristics of the fluvial and lacustrine record at Linás de Broto suggest a complex sedimentary evolution resulting from an expansion-retraction cycle of the lake, parallel to a retrogradation-progradation cycle of the high-energy braided fluvial system entering the lake (Fig. 11). This evolution implies changes in watershed hydrology, lake hydrology and sediment supply that were triggered by climate conditions in the context of the maximum glacier advance during the LGC in the south-central Pyrenees.

Deposition of Unit 1 was produced in shallow bars and channels in a high energy braided fluvial environment. This environment developed as a narrow outwash train in front of the Sorrosal glacier. Small gravelly and sandy deltaic lobes formed on the

ACCEPTED MANUSCRIPT

northern lakeshore areas (e.g., FA 2A). Most of this coarse sediment originated from melting of ice masses that dragged and transported till deposits of the Sorrosal glacier (Figs. 11, 12). Sediments were also derived from the hilly slopes throughout the valley. From clast composition (with very rare granite clasts carried by the Ara glacier from the Pyrenean Axial Zone), it can be deduced that only a very small proportion of sediments into the depositional system derived from the trunk Ara glacier via its lateral moraine (e.g., via ice sliding that would form icebergs in the lake). These processes imply a low water lake level (Fig. 12A), i.e., a lowering with respect to levels during deposition of Units 2 and 4 (Fig. 12B). The Viu moraine (A1 in Fig. 2B) was built, at least partially during Unit 1 deposition.

According to the age estimates obtained, the fluvial depositional phase of Unit 1 occurred before 55±9 ka BP, at the end of the MIS4 or very close to the MIS4-MIS3 transition (approximately at 59 ka after Martinson et al., 1987), considering the global boundaries between events provided by Lisiecki and Raymo (2005). In the valleys of the Cinca and Gállego rivers (Fig. 1), Lewis et al. (2009) linked fluvial aggradation phases during the mid-late Pleistocene to enhanced periods of glacier melting that produced massive discharges of water and sediment downstream along the valleys. These meltwater discharge processes were related to periods of maximum summer insolation during cold and transitions from cold to deglaciation phases (Lewis et al., 2009). High geomorphic significance can be attributed to the glacial stage at 64±11 ka, recorded in the terminal moraine of Salinas de Sin, in the Cinca/Cinqueta valley (MIS4; 4a in Fig. 1B), and the correlated Qt7 terrace in the River Cinca valley (4b in Fig. 1B) at 61±4 ka (Lewis et al., 2009). The relationship between increased fluvial aggradation

ACCEPTED MANUSCRIPT

and high summer insolation periods is also shown by Benito et al. (2010) in the River Gállego valley.

Thus, the deposition of Unit 1 in Linás de Broto could be related to this regional fluvial aggradational period. In this context, the deposits at Linás de Broto preserve a record of higher frequency changes: periods with high summer insolation (i.e., associated with an increase of alluvial sediment supply) and periods with reduced summer insolation (i.e., associated with a decrease of melting water). In this way, Units 3 and 5 of sections LB1 and LB2 (Fig. 3) represent short fluvial progradation phases (e.g., stage 3 in Fig. 11B) that may be related to periods of maximum summer insolation that provided low ratios of water discharge vs. sediment flux.

The deposits of Units 3 and 5 clearly indicate a southeastward progradation of the fluvial system that ended up with size reduction of the lake surface and maybe the final lake filling episode (Fig. 12A). Considering the age of Unit 2 (from 55±9 to 49±11 ka BP), the deposits of Units 3 to 5 were likely deposited during MIS3 (this stage lasted approximately from 59 to 24 ka, after Martinson et al., 1987). This MIS encompasses several global stadial phases (Rasmussen et al., 2014), as well as a general maximum summer insolation in the northern hemisphere (Berger and Loutre, 1991).

In contrast, deposits of Units 2 (55±9 to 49±11 ka BP) and 4 (Fig. 3) represent rapid expansion stages of the lake (e.g., as evidenced through sharp contact between underlying coarse deposits and fine sediments containing dropstones) and coincide with the retrogradation of the fluvial system (Figs. 11A, 12B). Structureless clays may record long periods without, or with only minor, coarse sediment supply to the

ACCEPTED MANUSCRIPT

expanded lake. These observations could be interpreted as a high ratio of water discharge vs. sediment flux. However, lake expansion was primarily caused by rapid and prolonged closure of the lake by the lateral moraine and ice growth of the Ara glacier, likely during relatively colder conditions, and probably coinciding with low-insolation summer periods. In this context, very fine, mostly rhythmic lamination and dropstones would form during relatively short (i.e., seasonal) climate fluctuations. However, the possibility that these laminites represent varves is ruled out because ice-contact lakes are not fully sensitive to seasonal changes in temperature (cf., Ashley, 2002). Moreover, the irregular variations of lamina thickness through time and abundance of turbidite-like deposits within the Linás de Broto offshore sequence support non-seasonal/non-periodic sediment inputs to the lake.

Given the different deposition rates inferred from the sedimentary attributes (e.g., fluvial and deltaic deposits versus laminites) of Units 1, 3 and 5 compared to Units 2 and 4, it can be suggested that the deposition of gravelly sediments or fluvial progradation occurred during short periods characterized by dominant high summer insolation, which favored ablation and sediment production. In contrast, lake expansion occurred during longer periods with dominant low summer insolation, which decreased ablation and sediment production. This sedimentary scenario was made possible as a consequence of lake closure by the Ara trunk glacier.

6.2. Palaeoclimatic implications: the maximum ice extent during the Last Glacial Cycle in the Pyrenees

ACCEPTED MANUSCRIPT

The timing of the maximum ice extent through the LGC (130-14 ka, according Gibbard and Cohen, 2008) and the occurrence of the LGM (≈ 23-19 ka, according Hughes et al., 2013) in the south Pyrenees have been persistent matters of debate. Indirect dates from lacustrine records (Montserrat-Martí, 1992; García-Ruiz et al., 2003; González-Sampériz et al., 2006), and optically stimulated luminescence (Sancho et al., 2003; Lewis et al., 2009; García-Ruiz et al., 2013) and terrestrial cosmogenic nuclides (TCN) dates (Delmas et al., 2008; Pallás et al., 2010; Calvet et al., 2011) confirmed the asynchronous nature of the regional maximum glacier advances in respect to global glaciations.

In this work, the occurrence of a maximum ice extent of the Ara glacier prior to 51±9 ka (age from the three reliable OSL dates; Table 2) during the LGC has been reported. It has a regional expression that is documented in the different south-central Pyrenean glaciated valleys (e.g., points with datings in Fig. 1B, Table 3). Of these, the terminal till of Salinas de Sin (point 4a in Fig. 1B), gave an OSL age of 64±11 ka (Sancho et al., 2003, 2004; Lewis et al., 2009). In the Sabiñánigo sector of the River Gállego valley, extensive fluvio-glacial terraces (point 2b in Fig. 1B) yielded OSL ages ranging between 62.7±3.9 and 69±8 ka (the preferred combined age is 68±7 ka; Peña et al., 2004; Lewis et al., 2009). A terminal moraine at Castiello de Jaca (River Aragón valley, also to the west of the River Ara valley; point 1b in Fig. 1B) showed an OSL age of 68±7 ka (García Ruiz et al., 2013).

Farther east, using ^{10}Be exposure ages, Pallàs et al. (2010) found that the maximum glacial extent in some eastern Pyrenean valleys (e.g. Carol and Malnuy valleys) may have occurred during MIS4 (approximately 74-59 ka, after Martinson et al., 1987).

ACCEPTED MANUSCRIPT

Similarly, in the River Valira valley, Andorra (point 5 in Fig. 1B), Turu et al. (2017) placed the Würmian maximum ice extent at 59±1.18 ka, an age obtained from cosmogenic isotope analyses applied to a glacially-polished rock surface. Nevertheless, Pallás et al. (2006), using also exposure ages on boulders and glacial erosion landforms, indicated that pleniglacial conditions in the eastern Pyrenees could have occurred over a long period (from 30 to 20 ka), including several glacier advances and retreats, with a last maximum glacier advance during the LGM (≈ 18 ka ago). Delmas et al. (2008), by using cosmogenic dates, also reported the maximum ice advance to have occurred during the LGM in the eastern Pyrenees. Calvet et al. (2011) and Delmas et al. (2011) also confirmed the asynchroneity of the maximum ice extent during the LGC in the Pyrenees.

Thus, the maximum ice extent during the LGC in the central Pyrenees is older than LGM, whereas in the eastern Pyrenees it occurred later, coinciding with the LGM. Consequently, a non-uniform behaviour represented by the extent of glaciers, both from Northern Europe to Iberian Peninsula (latitudinal/global scale) and from west to east along the Pyrenees (longitudinal/regional scale) could be stated.

It is not easy to explain this asynchronous global and regional nature of the maximum glacier advances during the LGM at the Pyrenees. The different latitudinal response of the Pyrenean glacial systems respect to the northernmost continental ice-sheets (e.g., Ehlers and Gibbard, 2004) may be explained by the southern latitude of the Pyrenees (Florineth and Schlüchter, 2000; García-Ruiz et al, 2003). Low-latitude climate in the southern North-Atlantic appears to be very sensitive to the latitudinal shifts of the Polar Front controlling the westerlies regime in the North Atlantic (Calvo et al., 2001;

ACCEPTED MANUSCRIPT

Eynaud et al., 2009; Domínguez-Villar et al., 2013). A southernmost position of the Polar Front during the LGM (MIS2), located between 37°N and 43°N (Calvo et al., 2001), would restrict the advance of the south-central Pyrenean glaciers due to the decreased precipitation (Florineth and Schlüchter, 2000; Sanchez-Goñi et al., 2008), probably associated with the low sea-surface temperature in comparison with other periods (Domínguez-Villar et al., 2013). Consequently, cold and arid conditions prevailed during the LGM in the Pyrenees, as deduced from palynological records (Jalut et al., 1992). However, discrepancies about the position of the Polar Front and the derived sea-surface temperature have been observed. For example, Eynaud et al. (2009) indicate that the Polar Front did not reach the Iberian Peninsula during the LGM and a northward advance of warm waters is proposed.

Latitudinal migrations of the Polar Front during LGM affecting the western Iberian margin imply changes in the sea surface temperature (SST). But, controversy also appears when SSTs are estimated. Calvo et al. (2001) indicate SSTs of 8-10°C at 43°N during the LGM. SSTs of 2 to 4°C lower than at present have been reconstructed by Waelbroeck et al. (2014). However, this difference is lower (≈ 1 to 2°C) according to Eynaud et al. (2009). Regardless, this difference is minimal for mean estimated summer SST at 43°N in the western Iberian margin (present is 17.8°C, and LGM estimate is 17.4°C) (Salgueiro et al., 2010).

The asynchronous regional extent of glaciers from central to eastern Pyrenees could be related to the increase of snow precipitations in the eastern Pyrenean sector, compatible with a more southerly position of the Polar Front, but also consistent with a strengthening of the low pressure systems in a warmer western Mediterranean sea

ACCEPTED MANUSCRIPT

compared to a cooler southern North-Atlantic ocean during the LGM (Delmas et al., 2011). Delmas et al. (2011), based on temperature reconstructions from diverse proxies by Hayes et al. (2005) and de Vernal et al. (2005), suggest mean annual SSTs of 13-14.5°C in the Balearic area, and of 6.3-7.6°C in the Bay of Biscay. Other reconstructions of SSTs during the LGM in the western Iberian margin and the western Mediterranean show an attenuation of the temperature gradient between these areas due to a reorganization of surface water circulation in the western Mediterranean and a reduction in the inflow of Atlantic water (Waelbroeck et al., 2014).

7. Conclusions

The geomorphology, stratigraphy and sedimentology, along with chronology of the glacio-fluvio-lacustrine sequence at Linás de Broto (south-central Pyrenees, Northeastern Iberian Peninsula) allow us to characterize the evolution of the depositional system as well as to derive regional climate implications for late Pleistocene.

1) The sequence, ≈ 55 m thick, is divided into five lithological units that formed in three main environments: gravel braided system (outwash train), lake margin (gravel and sand deltas and fans) and distal lake or lake bottom plain (e.g., rhythmites, from distal hyperpycnal flows and dominant settling from suspension). Twelve facies associations represent the sedimentation variations through time in these settings.

2) The age estimates obtained within the middle portion of the sequence (Unit 2) range from 55±9 ka to 49±11 ka. Thus, the sequence developed during MIS4 and, partially, MIS3. The occurrence of this depositional system is related to the maximum

ACCEPTED MANUSCRIPT

ice extent of the Ara trunk glacier during the Last Glacial Cycle. These dates confirm the early age (during MIS4) of the maximum ice extent of the south-central Pyrenean glaciers. The asynchronous response of the Pyrenean glacial systems respect to Northern Europe glaciers seems related to the position of the Polar Front in the western Iberian margin through its influence on precipitation during the LGM.

3) The evolution of the studied environments over the period of maximum ice extent in the south-central Pyrenees is consistent with a complex expansion-retraction lacustrine stage that paralleled a complex retrogradation-progradation stage of the fluvial system. Fluvial progradation may be related to short periods of ice melting, while lake expansion concurred with ice-dam growth in the trunk glacier during longer periods. Thus, the development of proglacial, glaciolacustrine environments can be sensitive to variations in summer insolation regulated by orbital forcing.

Acknowledgments

This study is a contribution of the research groups *Paleoambientes del Cuaternario*, *Análisis de Cuencas Sedimentarias Continentales* and *Geomorfología y Cambio Global* (Aragon Government and European Social Fund) and of the Environmental Sciences Institute of the University of Zaragoza (IUCA). The authors would like to thank he *Servicios de Apoyo a la Investigación* (SAI) of the University of Zaragoza (Spain). An anonymous reviewer and editor Dr. Knight helped improve the manuscript.

References

Allen, J.R.L., 1970. A quantitative model of climbing ripples and their cross-laminated deposits. Sedimentology 14, 5-26.

ACCEPTED MANUSCRIPT

Allen, J.R.L., 1971. Instantaneous sediment deposition rates deduced from climbing ripple cross-lamination. Journal of the Geological Society of London 127, 553-561.

Allen, J.R. 1982a. Sedimentary structures: their character and physical basis, volume I. Developments in Sedimentology 30A, Elsevier, Amsterdam, 593 pp.

Allen, J.R. 1982b. Sedimentary structures: their character and physical basis, volume II. Developments in Sedimentology 30B, Elsevier, Amsterdam, 663 pp.

Allen, P.A., 1981. Sediments and processes on a small stream-flow dominated, Devonian alluvial fan, Shetland Islands. Sedimentary Geology 29, 31-66.

Arenas, C., Pardo, G., González, A., Villena, J., 1989. El sistema aluvial de Cobatillas (Teruel): análisis de facies y evolución del estilo fluvial. Revista de la Sociedad Geológica de España 2, 41-54.

Ashley, G.M., 2002. Glaciolacustrine environments. In: Menzies, J. (Ed.), Modern and Past Glacial Environments. Butterworth-Heinemann, Oxford, pp. 335-359.

Barnolas, A., Pujalte, V., 2004. La Cordillera Pirenaica. In: Vera, J.A. (Ed.), Geología de España. Sociedad Geológica de España-Instituto Geológico y Minero de España, Madrid, pp. 233-241.

Barrere, P., 1963. La période glaciaire dans l'Ouest des Pyrénées centrales Franco-espagnoles. Bulletin de la Société Géologique de France 7, 516-526.

ACCEPTED MANUSCRIPT

Benito, G., Sancho, C., Peña, J.L., Machado, M.J., Rhodes, E.J., 2010. Large-scale karst subsidence and accelerated fluvial aggradation during MIS6 in NE Spain: climatic and paleohydrological implications. Quaternary Science Reviews 29, 2694-2704.

Berger, A., Loutre, M.F., 1991. Insolation values for the climate of the last 10 million years. Quaternary Science Reviews 10, 297-317.

Blair, T.C., 1987. Sedimentary processes, vertical stratification sequences, and geomorphology of the Roaring River alluvial fan, Rocky Mountain National Park, Colorado. Journal of Sedimentary Petrology 57, 1-18.

Bordonau, J., 1992. Els complexos glàcio-lacustres relacionats amb el darrer cicle glacial als Pirineus. Geoforma Ediciones, Logroño, 251 pp.

Bordonau, J., Vilaplana, J.M., Fontugne, M., 1993. The glaciolacustrine complex of Llestui (Central Southern Pyrenees). A key locality for the chronology of the last glacial cycle in the Pyrenees. Comptes rendus l'Académie des Sciences de Paris Série II, 316, 807-813.

Calvet, M., Delmas, M., Gunnell, Y., Braucher, R., Bourlès, D., 2011. Recent advances in research on Quaternary glaciations in the Pyrenees. In: Ehlers, J., Gibbard, P.L., Hughes, P. (Eds), Quaternary Glaciations, Extent and Chronology, A Closer Look, Part IV. Developments in Quaternary Science 15. Elsevier, Amsterdam, pp. 127-139.

Calvo, E., Villanueva, J, Grimalt, J.O., Boelaert, A., Labeyrie, L., 2001. New insights into the glacial latitudinal temperature gradients in the North Atlantic. Results from $U^{K'}_{37}$

ACCEPTED MANUSCRIPT

sea surface temperatures and terrigenous inputs. Earth and Planetary Science Letters 188, 509-519.

Carrasco, R.M., Pedraza, J., Domínguez-Villar, D., Villa, J., Willenbring, J.K., 2013. The plateau glacier in the Sierra de Béjar (Iberian Central System) during its maximum extent. Reconstruction and chronology. Geomorphology 196, 83-93.

Carrasco, R.M., Pedraza, J., Domínguez-Villar, D., Willenbring, J.K., Villa, J., 2015. Sequence and chronology of the Cuerpo de Hombre paleoglacier (Iberian Central System) during the last glacial cycle. Quaternary Science Reviews 129, 163-177.

Cheel, R.J., Rust, B.R., 1986. A sequence of soft sediment deformation (dewatering) structures in late Quaternary subaqueous outwash near Ottawa, Canada. Sedimentary Geology 47, 77-93.

Chueca, J., Peña, J.L., Lampre, F., García-Ruiz, J.M., Martí-Bono, C., 1998. Los glaciares del Pirineo aragonés: estudio de su evolución y extensión actual. Departamento de Geografía y Ordenación del Territorio. Universidad de Zaragoza, 104 pp.

De la Riva, J., 2000. Caracterización climática del alto valle de Tena. Boletín Glaciológico Aragonés 1, 81-109.

de Vernal, A., Rossell-Melé, A., Kucera, M., Hillaire-Marcel, C., Eynaud, F., Weinelt, M., Dokken, T., Kageyama, M., 2005. Comparing proxies for the reconstruction of LGM sea-surface conditions in the northern North Atlantic. Quaternary Science Reviews 25, 2820-2834.

ACCEPTED MANUSCRIPT

Del Barrio, G., Creus, J., Puigdefábregas, J., 1990. Thermal seasonality of the high mountain belts of the Pyrenees. Mountain Research and Development 10, 227-233.

Delmas, M., Calvet, M., Gunnell, M., Braucher, R., Bourlès, D., 2011. Palaeogeography and ^{10}Be exposure-age chronology of Middle and Late Pleistocene glacier systems in the northern Pyrenees: implications for reconstructing regional palaeoclimates. Palaeogeography, Palaeoclimatology, Palaeoecology 305, 109-122.

Delmas, M., Gunnell, Y., Braucher, R., Calvet, M., Bourlès, D., 2008. Exposure age chronology of the last glaciation in the eastern Pyrenees. Quaternary Research 69, 231-241.

Desloges, J.R., 1994. Varve Deposition and the Sediment Yield Record at Three Small Lakes of the Southern Canadian Cordillera. Arctic and Alpine Research 26, 130-140.

Domínguez-Villar, D., Carrasco, R.M., Pedraza, J., Cheng, H., Edwards, R.L., Willenbring, J.K., 2013. Early maximum extent of paleoglaciers from Mediterranean mountains during the last glaciation. Scientific Reports 3, 2034, DOI: 10.1038/srep02034.

Ehlers, J., Gibbard, P.L. (Eds), 2004. Quaternary Glaciations. Extent and Chronology, Part I: Europe. Developments in Quaternary Science 2, Elsevier, London, 488 pp.

Evans, D.J.A., Rother, H., Hyatt, O.M., Shulmeister, J., 2013. The glacial sedimentology and geomorphological evolution of an outwash head/moraine-dammed lake, South Island, New Zealand. Sedimentary Geology 284-285, 45-75.

ACCEPTED MANUSCRIPT

Eyles, C.H., Eyles, N., 2010. Glacial Deposits. In: James, N.P., Dalrymple, R.W. (Eds.), Facies models 4, Series GEOtext 6. Geological Association of Canada, Canada, pp. 73-104.

Eynaud F., Abreu, L., Voelker, A., Schönfeld, J., Salgueiro, E., Turon, J.L., Penaud, A., Toucanne, S., Naughton, F., Sánchez-Goñi, M.F., Malaizé, B., Cacho, I., 2009. Position of the Polar Front along the western Iberian margin during key cold episodes of the last 45 ka. Geochemistry, Geophysics, Geosystems 10, DOI: 10.1029/2009GC002398.

Florineth, D., Schlüchter, Ch., 2000. Alpine evidence for atmospheric circulation patterns in Europe during the Last Glacial Maximum. Quaternary Research 54, 295-308.

Fuller, I.C., Macklin, M.G., Lewin, J., Passmore, D.G., Wintle, A.G., 1998. River response to high-frequency climate oscillations in southern Europe over the past 200 k.y. Geology 26, 275-278.

García, J.L., Jorge A. Strelin, J.A., Vega, R.M., Hall, B.L., Stern, C.R., 2015. Deglacial ice-marginal glaciolacustrine environments and structural moraine building in Torres del Paine, Chilean southern Patagonia. Andean Geology 42, 190-212.

García-Ruiz, J.M., Martí-Bono, C., 1994. Rasgos fundamentales del glaciarismo Cuaternario en el Pirineo aragonés. In: Martí-Bono, C., García-Ruiz, J.M. (Eds.), El glaciarismo surpirenaico: nuevas aportaciones. Geoforma Ediciones, Logroño, pp. 17-31.

ACCEPTED MANUSCRIPT

García-Ruiz, J.M., Valero-Garcés, B.L., Martí-Bono, C., González-Sempériz, P., 2003. Asynchroneity of maximum glacier advances in the central Spanish Pyrenees. Journal of Quaternary Science 18, 61-72.

García-Ruiz, J.M., Martí-Bono, C., Peña-Monné, J.L., Sancho, C., Rhodes, E.J., Valero-Garcés, B., González-Sampériz, P., Moreno, A., 2013. Glacial and fluvial deposits in the Aragón Valley, central-western Pyrenees: chronology of the Pyrenean late Pleistocene glaciers. Geografiska Annaler: Series A, Physical Geography 95, 15-32.

Gibbard, P., Cohen, K.M., 2008. Global chronostratigraphical correlation table for the last 2.7 million years. Episodes 31, 243-247.

González-Sampériz, P., Valero-Garcés, B. L., Moreno, A., Jalut, G., García-Ruiz, J.M., Martí-Bono, C., 2006. Climate variability in the Spanish Pyrenees during the last 30,000 yr revealed by the El Portalet sequence. Quaternary Research 66, 38-52.

Gruszka, B., 2001. Climatic versus tectonic factors in the formation of the glaciolacustrine succession (Bełchatów outcrop, central Poland). Global and Planetary Change 28, 53-71.

Gruszka, B., 2007. The Pleistocene glaciolacustrine sediments in the Bełchatów mine (central Poland): Endogenic and exogenic controls. Sedimentary Geology 193, 149-166.

Hayes, A., Kucera, M., Kallel, N., Sbaffi, L., Rohling, E.J. ,2005. Glacial Mediterranean sea surface temperatures based on planktonic foraminiferal assemblages. Quaternary Science Reviews 24, 999-1016.

ACCEPTED MANUSCRIPT

Hughes, P.D., Woodward, J.C., 2008. Timing of glaciation in the Mediterranean mountains during the last cold stage. Journal of Quaternary Science 23, 575-588.

Hughes, P.D., Gibbard, P.L., Ehlers, J., 2013. Timing of glaciation during the last glacial cycle: evaluating the meaning and significance of the 'Last Glacial Maximum' (LGM). Earth-Science Reviews 125, 171-198.

Hughes, P.D., Woodward, J.C., Gibbard, P.L., 2006a. Quaternary glacial history of the Mediterranean mountains. Progress in Physical Geography 30, 334-364.

Hughes, P.D., Woodward, J.C., Gibbard, P.L., 2006b. Late Pleistocene glaciers and climate in the Mediterranean. Global and Planetary Change 50, 83-98.

Jalut, G., Montserrat-Martí, J., Fontugne, M., Delibrias, G., Vilaplana, J.M., Julia, R., 1992. Glacial to interglacial vegetation changes in the northern and southern Pyrenees: Deglaciation, vegetation cover and chronology. Quaternary Science Reviews 11, 449-480.

Jiménez-Sánchez, M., Rodríguez-Rodríguez, L., García-Ruiz, J.M., Domínguez-Cuesta, M.J., Farias, P., Valero-Garcés, B., Moreno, A., Rico, M., Valcárcel, M., 2013. A review of glacial geomorphology and chronology in northern Spain: Timing and regional variability during the last glacial cycle. Geomorphology 196, 50-64

Johnsen, T.F., Brennand, T.A., 2006. The environment in and around ice-dammed lakes in the moderately high relief setting of the southern Canadian Cordillera. Boreas 35, 106-125.

ACCEPTED MANUSCRIPT

Jopling, A.V., Walker, R.G., 1968. Morphology and origin of ripple-drift cross lamination, with examples from the Pleistocene of Massachusetts. Journal of Sedimentary Petrology 38, 971-984.

Kostic, B., Becht, A., Aigner, T., 2005. 3-D sedimentary architecture of a Quaternary gravel delta (SW-Germany): Implications for hydrostratigraphy. Sedimentary Geology 181, 143-171.

Krzyszkowski, D., 1994. Controls on sedimentation in the Elsterian proglacial lake, Kleszczów Graben, central Poland. In: Warren, W.P., Croot, D.G. (Eds.), Formation and Deformation of Glacial Deposits. Balkema, Rotterdam, pp. 53-68.

Lewis, C., McDonald, E., Sancho, C., Peña, J.L., Rhodes, E., 2009. Climatic implications of correlated Upper Pleistocene glacial and fluvial deposits on the Cinca and Gállego Rivers (NE Spain) based on OSL dating ans soil stratigraphy. Global and Planetary Change 67, 141-152.

Lisiecki, L.E., Raymo, M.E., 2005. A Pliocene-Pleistocene stack of 57 globally distributed benthic $\delta^{18}O$ records. Paleoceanography 20, PA1003, doi:10.1029/2004PA001071.

López, F., Cabrera, M., Cuadrat, J.M., 2007. Atlas Climático de Aragón. Departamento de Medio Ambiente, Gobierno de Aragón, España, 213 pp.

Mallada, L., 1878. Descripción física y geológica de la provincia de Huesca. Memorias de la Comisión del Mapa Geológico de España, Madrid, 432 pp., 1 mapa.

Martí-Bono, C., 1977. El valle de Hecho. Trabajos sobre Neógeno-Cuaternario 6, 349-356.

ACCEPTED MANUSCRIPT

Martí-Bono, C., 1996. El glaciarismo cuaternario en el Alto Aragón Occidental. PhD Thesis, Universitat de Barcelona, 254 pp.

Martí-Bono, C., González-Sampériz, P., Valero-Garcés, B., García-Ruiz, J.M., 2002. El depósito glaciolacustre de Linás de Broto (Pirineo aragonés) y su implicación paleoambiental. In: Pérez-González, A., Vegas, J., Machado, M.J. (Eds.), Aportaciones a la Geomorfología de España en el inicio del Tercer Milenio. Instituto Geológico y Minero de España, pp. 77-83.

Martinson, D.G., Pisias, N.G, Hays, J.D., Imbrie, J., Moore, T.C., Shackleton, N.J., 1987. Age dating and the orbital theory of the ice ages: Development of a high-resolution 0 to 300,000-year chronostratigraphy. Quaternary Research 27, 1-29.

Matthews, J.A., Dahl, S.O., Nesje, A., Berrisford, M.S., Andersson, C., 2000. Holocene glacier variations in central Jotunheimen, southern Norway based on distal glaciolacustrine sediment cores. Quaternary Science Reviews 19, 1625-1647.

Miall, A.D., 1977. A review of the braided river depositional environment. Earth-Science Reviews 13, 1-62.

Miall, A.D., 1978. Lithofacies types and vertical profile models in braided river deposits: a summary. In: Miall, A.D. (Ed.), Fluvial Sedimentology. Canadian Society of Petroleum Geologists Memoir 5, pp. 597–604.

Montserrat-Martí, J.M., 1992. Evolución glaciar y postglaciar del clima y la vegetación en la vertiente sur del Pirineo: Estudio palinológico. Monografías del IPE, Instituto Pirenaico de Ecología (CSIC), Zaragoza, España, vol. 6, 147 pp.

ACCEPTED MANUSCRIPT

Monserrat, J.M., Vilaplana, J.M., 1988. The paleoclimatic records of the Upper Pleistocene and Holocene in the Llauset Valley (Central Pyrenees). Pirineos 129, 107-113.

Mulder, T., Alexander, J., 2001. The physical character of subaqueous sedimentary density flows and their deposits. Sedimentology 48, 269-299.

Muñoz, J.A., 2002. The Pyrenees. In: Gibbons, W, Moreno, T. (Eds.), The geology of Spain. Geological Society, London, pp. 370-385.

Murray, A.S., Wintle, A.G., 2000. Luminiscence dating of quartz using an improved single-aliquot regenerative-dose protocol. Radiation Measurements 32, 57-73.

Murray, A.S., Wintle, A.G., 2003. The single aliquot regenerative dose protocol: potential for improvements in reliability. Radiation Measurements 37, 377-381.

Nussbaum, F., 1946. Orographische und morphologische untersuchungen in den Ostlichen Pyrenäen. Jahresberichtr der Geographischen Gesellschaft von Bern XXV-XXVI, 247 pp.

Palacios, D., Gómez-Ortiz, A., Andrés, N., Vázquez-Selem, L., Salvador-Franch, F., Oliva, M., 2015. Maximum extent of Late Pleistocene glaciers and last deglaciation of La Cerdanya mountains, Southeastern Pyrenees. Geomorphology 231, 116-129.

Palacios, D., Marcos, J., Vázquez-Selem, L., 2011. Last Glacial Maximum and deglaciation of Sierra de Gredos, central Iberian Peninsula. Quaternary International 233, 16-26.

ACCEPTED MANUSCRIPT

Pallás, R., Rodés, A., Braucher, R., Carcailler, J., Ortuño, M., Bordonau, J., Bourlés, D., Vilaplana, J.M., Masana, E., Santanach, P., 2006. Late Pleistocene and Holocene glaciation in the Pyrenees: a critical review and new evidence from ^{10}Be exposure ages, south-central Pyrenees. Quaternary Science Reviews 25, 2937-2963.

Pallás, R., Rodés, A., Braucher, R., Bourlès, D., Delmas, M., Calvet, M., Gunnell, Y., 2010. Small, isolated glacial catchments as priority target for cosmogenic surface dating of Pleistocene climate fluctuations, SE Pyrenees. Geology 38, 891-894.

Panzer, W., 1926. Talentwicklung und Eiszeitklima in nordöstlichen Spanien. Abhandlungen der Senckenberg Naturforschung Gesellschaft 39, 141-182.

Penck, A., 1883. Die Eiszeit in der Pyrenaen. Mitt. Ver. Erdk. Leipzig. (Translated to French: La période glaciaire dans les Pyrénées. Bulletin de la Société d'Histoire Naturelle de Toulouse 19, 105-200.

Peña, J.L., Sancho, C., Lewis, C., McDonald, E., Rhodes, E., 2004. Datos cronológicos de las morrenas terminales del glaciar del Gállego y su relación con las terrazas fluvioglaciares (Pirineo de Huesca). In: Peña, J.L., Longares, L.A., Sánchez, M. (Eds.), Geografía Física de Aragón: aspectos generales y temáticos. Universidad de Zaragoza - Institución Fernando el Católico (CSIC), Zaragoza, España, pp. 71-84.

Pietras, J.T., Carrol, A.L., 2006. High-Resolution Stratigraphy of an Underfilled Lake Basin: Wilkins Peak Member, Eocene Green River Formation, Wyoming, U.S.A. Journal of Sedimentary Research 76, 1197–1214.

ACCEPTED MANUSCRIPT

Prior, D.B., Bornhold, B.D., 1988. Submarine morphology and processes of fjord fan deltas and related high gradient systems: modern examples from British Columbia. In: Nemec, W., Steel, R.J. (Eds.), Fan Deltas: Sedimentology and Tectonic Settings. Blackwell, London, pp. 125–143.

Rasmussen, S.O., Bigler, M., Blockley, S.P., Blunier, T., Buchardt, S.L., Clausen, H.B., Cvijanovic, I., Dahl-Jensen, D., Johnsen, S.J., Fischer, H., Gkinis, V., Guillevic, M., Hoek, W.Z., Lowe, J.J., Pedro, J.B., Popp, T., Seierstad, I.K., Steffensen, J.P., Svensson, A.M., Vallelonga, P., Vinther, B.M., Walker, M.J.C., Wheatley, J.J., Winstrup, M., 2014. A stratigraphic framework for abrupt climatic changes during the Last Glacial period based on three synchronized Greenland ice-core records: refining and extending the INTIMATE event stratigraphy. Quaternary Science Reviews 106, 14-28.

Reineck, H.E., Singh, I.B., 1980. Depositional sedimentary environments, second edition. Springer-Verlag, Berlin Heidelberg, 549 pp.

Rhodes, E.J., 1988. Methodological considerations in the optical dating of quartz. Quaternary Science Reviews 7, 395-400.

Rhodes, E.J., 2000. Observations of thermal transfer OSL signals in glacigenic quartz. Radiation Measurements 32, 595-602.

Rhodes, E.J., Pownall, L., 1994. Zeroing of the OSL signal in quartz from young glaciofluvial sediments. Radiation Measurements 23, 329-333.

Rhodes, E.J., Schwenninger, J.L., 2007. Dose rates and radioisotope concentrations in the concrete calibration blocks at Oxford. Ancient TL 25, 5-8.

ACCEPTED MANUSCRIPT

Ríos, L.M., Lanaja, J.M., Frutos, E., 1982. Mapa Geológico de España 1:50,000, hoja 178 (Broto). Instituto Geológico y Minero de España, Madrid, 60 pp.

Rodríguez-Rodríguez, L., Jiménez-Sánchez, M., Dominenguez-Cuesta, M.J., Rinterknecht, V., Pallàs, R., Bourlès, D., 2016. Chronology of glaciations in the Cantabrian Mountains (NW Iberia) during the Last Glacial Cycle based on in situ-produced ^{10}Be. Quaternary Science Reviews 138, 31-48.

Salgueiro, E., Voelker, A.H.L., de Abreu, L., Abrantes, F., Meggers, H., Wefer, G., 2010. Temperature and productivity changes off the western Iberian margin during the last 150 ky. Quaternary Science Reviews 29, 680-695.

Sánchez-Goñi, M.F., Landais, A., Fletcher, W.J., Naughton, F., Desprat, S., Duprat, J., 2008. Contrasting impacts of Dansgaard–Oeschger events over a western European latitudinal transect modulated by orbital parameters. Quaternary Science Reviews 27, 1136-1151.

Sancho, C., Peña, J.L., Lewis, C., McDonald, E., Rhodes, E., 2003. Preliminary dating of glacial and fluvial deposits in the Cinca River Valley (NE Spain): chronological evidences for the Glacial Maximum in the Pyrenees? In: Ruiz, M.B., Dorado, M., Valdeolmillos, A., Gil, M.J., Bardají, T., Bustamante, I., Martínez, I. (Eds.), Quaternary climatic changes and environmental crises in the Mediterranean region. Universidad de Alcalá-Ministerio de Ciencia y Tecnología-INQUA, pp. 169-173.

Sancho, C., Peña, J.L., Lewis, C., McDonald, E., Rhodes, E., 2004. Registros fluviales y glaciares cuaternarios en las cuencas de los ríos Cinca y Gállego (Pirineos y depresión del Ebro). In: Colombo, F., Liesa, C.L., Meléndez, G., Pocoví, A., Sancho, C., Soria, A.R.

ACCEPTED MANUSCRIPT

(Eds), Itinerarios Geológicos por Aragón. Geo-Guías 1, Sociedad Geológica de España, pp. 181-205.

Sancho, C., Peña-Monné, J.L., Rhodes, E., Arenas, C., Pardo, G., García-Ruiz, J.M., Martí-Bono, J.L., 2011. El registro glaciolacustre de Linás de Broto (Valle del Ara, Pirineo central, Huesca): nuevas aportaciones. In: Turu, V., Constante, A. (Eds.), El Cuaternario en España y áreas afines, avances en 2011. Resúmenes XIII Reunión Nacional de Cuaternario, Andorra, pp. 11-14.

Sancho, C., Calle, M., Peña-Monné, J.L., Duval, M., Oliva-Urcia, B., Pueyo E.L., Benito, G., Moreno, A., 2016. Dating the Earliest Pleistocene alluvial terrace of the Alcanadre River (Ebro Basin, NE Spain): Insights into the landscape evolution and involved processes. Quaternary International 407, 86-95.

Serrano, E., 1998. Geomorfología del Alto Gállego. Pirineo aragonés. Institución Fernando El Católico (CSIC), Zaragoza, España, 501 pp.

Serrano, E., Martínez de Pisón, E., 1994. Geomorfología y evolución glaciar en el Pirineo aragonés oriental. In: Martí-Bono, C., García-Ruiz, J.M. (Eds.), El glaciarismo surpirenaico: nuevas aportaciones. Geoforma Ediciones, Logroño, España, pp. 33-64.

Serrat, D., Vilaplana, J.M., Martí-Bono, C., 1982. Some depositional models in glaciolacustrine environments (southern Pyrenees). In: Evenson, E.B., Schlüchter, Ch., Rabassa, J. (Eds.), Tills and related deposits. Balkema, Rotterdam, pp. 231-244.

Shulmeister, J., Thackray, G.D., Rieser, U., Hyatt, O.M. Rother, H., Smart, C.C., Evans, D.J.A., 2010. The stratigraphy, timing and climatic implications of glaciolacustrine

ACCEPTED MANUSCRIPT

deposits in the middle Rakaia Valley, South Island, New Zealand. Quaternary Science Reviews 29, 2362-2381.

Smith, L.N., 2017. Repeated sedimentation and exposure of glacial Lake Missoula sediments: A lake-level history at Garden Gulch, Montana, USA. Quaternary Science Reviews 155, 114-126.

Stanley, K.O., 1974. Morphology and hydraulic significance of climbing ripples with superimposed micro-ripple-drift cross-lamination in Lower Quaternary lake silts, Nebraska. Journal of Sedimentary Petrology 44, 472-483.

Turu, V., 2002. Análisis secuencial del delta de Erts. Estratigrafía de un valle glaciar obturado intermitentemente, relación con el último ciclo glaciar. Valle de Arinsal, Pirineos Orientales. In: Estudios recientes (2000-2002) en geomorfología, patrimonio, montaña y dinámica territorial. Sociedad Española de Geomorfología-Universidad de Valladolid, España, pp. 565-574.

Turu, V., Calvet, M., Bordonau, J., Gunnell, Y., Delmas, M., Vilaplana, J.M., Jalut, G., 2017. Did Pyrenean glaciers dance to the beat of global climatic events? Evidence from the Würmian sequence stratigraphy of an ice-dammed paleolake depocentre in Andorra. In: Hughes, P.D., Woodward, J.C. (Eds.), Quaternary glaciation in the Mediterranean mountains. Geological Society of London, Special Publications 433, pp. 111-136.

Vera, J.A. (Ed.), 2004. Geología de España. Sociedad Geológica de España-Instituto Geológico y Minero de España, Madrid, 890 pp.

ACCEPTED MANUSCRIPT

Vilaplana, J.M., 1983. Estudi del glaciarisme quaternari de les altes valls de la Ribagorça. PhD Thesis. Universitat de Barcelona, 322 pp.

Vilaplana, J.M., Monserrat, J., Schluchter, Ch., 1989. Recent progress in Quaternary stratigraphy: the Lake Llauset sequences in the Spanish Pyrenees. In: Rose, J., Schluchter, Ch. (Eds.), Quaternary type sections: imagination or reality? Balkema, Rotterdam, pp. 123-134.

Vilaplana, J.M., Schluchter, Ch., Verdaguer, A., 1983. Sedimentology and stratigraphy of the Pleistocene sediments in Lake Llauser (Southern Pyrenees, Spain). A first approach. Acta Geológica Hispánica 18, 235-248.

Waelbroeck, C., Kiefer, T., Dokken, T., Chen, M.-T., Spero, H.J., Jung, S., Veinelt, M., Kucera, M., Paul, A. on behalf of MARGO Project Members, 2014. Constraints on surface seawater oxygen isotope change between the Last Glacial Maximum and the Late Holocene. Quaternary Science Reviews 105, 102-111.

Wang, X., Vanderberghe, J., Shuangwen, Y., Van Balen, R., Lu, H., 2015. Climate-dependent fluvial architecture and processes on a suborbital timescale in areas of rapid tectonic uplift: An example from the NE Tibetan Plateau. Global and Planetary Change 133, 318-329.

Winsemann, J., Asprion, U., Meyer, T., 2007. Facies characteristics of Middle Pleistocene (Saalian) ice-margin subaqueous fan and delta deposits, glacial Lake Leine, NW Germany. Sedimentary Geology 193, 105–129.

ACCEPTED MANUSCRIPT

FIGURE AND TABLE CAPTIONS

Figure 1. (A) Location of the studied area. (B) Geologic setting adapted from Mapa Geológico de España, 1:2,000,000 (Vera, 2004). Sites with Pleistocene glacial and fluvial records relevant to this study: 1a: River Aragón (Castiello de Jaca, terrace; García Ruiz et al., 2013); 1b: River Aragón (Castiello de Jaca, moraine; García Ruiz et al., 2013). 2a: River Gállego (Senegüé, moraine; Lewis et al., 2009); 2b: River Gállego (Sabiñánigo, fluvio-glacial terrace; Lewis et al., 2009); 2c: River Gállego (Murillo de Gállego, terrace; Lewis et al., 2009). 3: River Ara (Asín de Broto, moraine; Serrano and Martínez de Pisón, 1994). 4a: River Cinca (Salinas de Sin, moraine; Sancho et al. 2003, 2004; Lewis et al., 2009); 4b: River Cinca (El Grado, terrace Qt8; Lewis et al., 2009); 4c: River Cinca (Alfántega, terrace Qt7; Lewis et al., 2009). 5: River Valira (Andorra, moraines; Turu et al., 2017). 6: Ariège valley (northeastern Pyerenees, France, moraines; Delmas et al., 2011).

Figure 2. (A) Geomorphologic map of the studied area. Sorrosal glacier moraines: S1, S2 and S3. (B) Detailed map of the Linás de Broto area, with location of stratigraphic sections LB1 and LB2. In A and B, Ara glacier moraine at Viu: A1.a, A1.b and A.1c. A.1c is a kame terrace (with no morphological expression at map scale); Ara glacier moraine at Fragen: A2. (C) Reconstruction of the maximum glacier extension of the Ara glacier during the Last Glacial Cycle (based on Serrano and Martínez de Pisón, 1994; Martí-Bono, 1996).

Figure 3. Stratigraphic sections measured in the River Sorrosal valley (location in figure 2B). Section LB1 is adapted from Sancho et al. (2011). Correlation is based on physical

ACCEPTED MANUSCRIPT

continuity of sedimentary surfaces (e.g., gravel beds) in the field. Facies nomenclature in Table 1 and facies associations in Figure 10.

Figure 4. (A) Panoramic view of the Linás de Broto outcrop, with location of the two stratigraphic sections and correlation of units based on continuity of sedimentary surfaces and lithological composition. (B) Field image that shows a portion of Unit 1, with the lowermost sand and gravel outcrop.

Figure 5. Field views of sedimentary facies (gravels) and facies associations. See Table 1 for nomenclature and features of facies and Figure 10 for facies associations. (A, B) Structureless (Gm) and horizontal-stratified (Gh) clast-supported gravels and horizontal-laminated sands (Sh), arranged as FA 1. (C) Detail of structureless clast-supported gravels (Gm), with rip-up clasts (arrowed) and interbedded thin sand interval (facies Sh). (D) Structureless sandy-rich, clast-supported gravels (Gm, in FA 1B). (E) Erratic clast (≈ 0.5 m long) in Unit 1. (F) Foreset cross-stratification in gravels (Gf) and sands (Sf) in FA 2A, and overlying structureless clast-supported gravels. (G) Detail of foreset cross-stratification, underlying sands with ripples (facies Sr2) and horizontal lamination (facies Sh). (H) Detail of gravel and sand wedges at the distal termination of foresets in facies Gf and Sf.

Figure 6. Field views of sedimentary facies (sand and silt) and facies associations. See Table 1 for nomenclature and features of facies and Figure 10 for facies associations. (A) Sands of Unit 2, structureless (facies Sm), with horizontal lamination (Sh) and in-phase climbling ripple lamination (Sr1) (FA 2A), underlying structureless gravels (Gm) of Unit 3. (B) In-phase and in-drift climbling ripple lamination (Sr1) in sands of Unit 2.

ACCEPTED MANUSCRIPT

(C) In-drift climbing ripple lamination (Sr1) in sands of Unit 2. (D) In-drift climbing ripple lamination (Sr1) and structureless (Sm) sands of Unit 2. (E) Sands with horizontal lamination (Sh) and scour and fill (Ss) stratification, underlying cross-stratified sands and gravels (St, Gt), forming FA 2C. (Unit 2). (F) Foreset cross-stratification in sands and minor gravels (Sf, Gf), overlying sands with horizontal and ripple lamination (Sh, Sr1 and Sr2) of Unit 1 (section LB-1), arranged as FA 2A. Note overlying structureless gravels of Unit 3. (G) Assymmetric ripples (Sr2) and structureless sand with erratics (Sm) at the base of a coarsening upward sequence (FA 2A) underlying Unit 1.

Figure 7. Field views of sedimentary facies (silt and clay) and lacustrine facies associations. See Table 1 for nomenclature and features of facies and Figure 10 for facies associations. (A) Ripple cross-laminated silts (Fr), horizontal-laminated sand (Sh) and gravel (Gh), and structureless gravel (Gm), arranged in a coarsening upward sequence (FA 3A). (B) Alternating structureless gravel (Gm) and laminated and structureless clays (Clh, Clm) forming FA 4A. (C) Structureless and horizontal-laminated silts (Fm, Fh) and clays (Clh) forming FA 4B. (D) Alternating structureless silts and sands (Fm, Sm) and horizontal-laminated clays (Clh), representing FA 6A. (E) Alternating structureless silts and clays (Fm, Clm) and horizontal-laminated clays (Clh), representing FA 6B. (F) Detail of structureless and laminated clays containing dropstones (FA 6B).

Figure 8. Photomicrographs (A, B, D, optical microscope; C, scanning electron microscope, SEM) of horizontal-laminated mudstones that consist of clay laminae and thin silt interlaminae and interlenses (facies Clh). (A , B) Sharp basal contacts and fining upward as far as the following silt interval. (C) Detail of fining-upward evolution of a

ACCEPTED MANUSCRIPT

lamina (C: calcite; Q: quartz). (D) Dropstones, and deformed and undulate laminae. (A to D), the coarser grains are of quartz, calcite, and minor dolomite, rutile, apatite, iron oxides and pyrite; the finest particles mostly correspond to chlorite/clinochlore and muscovite (determined by XRD analysis and SEM microanalyses).

Figure 9. Field views of deformation structures. (A) Irregular folds in sand and gravel beds of Units 1 and 2. (B) Acute folds in sand beds of Unit 2. (C) Clay injections (flames) within fine sand bed (arrow at the bottom) and micrograben in horizontal-laminated sands bed (arrows). (D) Gently deformed lamination in clays and silts. (E, F) Clay injections (mushroom-shaped, cream and pale yellow in colour; arrows) within silt and fine sand laminated layers of Unit 2.

Figure 10. Facies associations formed in fluvial, deltaic and lacustrine environments. Explanation in the text. Nomenclature and summary of main features of the sedimentary facies are given in Table 1.

Figure 11. Sedimentary facies model for an ice-dammed lake (trunk glacier-valley ponded lake) that receives sediment supply through an outwash train fed by meltwater from a small glacier developed in the headwater of the tributary River Sorrosal valley. (A) Expansion of the lake, illustrated by stage 2 (as an example of the depositional settings of Units 2 and 4). (B) Progradation of fluvial streams and reduction of the lake during warmer periods, with outflow through former moraine dam, illustrated by stage 3 (as an example of the depositional settings of Units 1, 3 and 5).

ACCEPTED MANUSCRIPT

Figure 12. Two main stages of development of the glaciofluvial and glaciolacustrine system in the Linás de Broto ice-dammed lake: (A) Progradation of the braided fluvial system during warmer conditions, with reduction (or final disappearance) of lake surface (Units 1, 3 and 5). (B) Expansion of the lake due to closure by moraine and ice growth of the trunk glacier, with retrogradation of the fluvial braided system, during colder conditions (Units 2 and 4).

ACCEPTED MANUSCRIPT

ACCEPTED MANUSCRIPT

Table 1. Sedimentary facies and their interpretation in the Pleistocene deposits studied at Linás de Broto area.

Lithology	Texture and geometry of deposits	Sedimentary Facies	Interpretation: processes and depositional settings
Gravels. Figs. 4B, 5, 6F, 7A.	Grey to brown in colour. Clast-supported fabric. Polymictic clasts, mostly of brown to grey sandstones and dark grey limestones (from Palaeocene-Illerdian units and Eocene Hecho Group), and very rare granite clasts; commonly heterometric, from a few cm to 35 cm, apart from erractics than can reach up to 1.2 m in length; varied in shape and from poorly rounded to subrounded. Granule and sand matrix and very minor calcareous cement. Generally thick, up to 3 m, tabular bodies with crude stratification, and planar or wide concave bases. Locally, wedge- and lense-shaped bodies up to 1 m thick.	**Gm**: structureless, with rip-up clasts, fining-upward, coarsening upward or without size vertical trend. Figs. 4B, 5A, 5B, 5C, 5D, 5E. **Gh**: horizontal stratification, with or without clast imbrication. Folds. Figs. 5A, B, E, 9A. **Gp**: planar cross-stratification, sets dm thick. **Gt:** through cross-tratification, sets dm thick. **Gf:** foreset cross-stratification. Wedge- and lense-shaped (sigmoid) bodies dm thick. Figs. 4B, 5F, 5G, 5H.	Gm: Flash flood deposits and bar cores in braided fluvial context (Miall, 1978, 2000; Arenas et al., 1989). Deposition from a high-velocity expanding jet onshore and offshore (Ashley, 2002). Deposition in longitudinal bars of braided fluvial systems (Gh<> Sh) (Miall, 1978; Arenas et al., 1989). Deposition in transverse bars and crescent dunes in shallow braided channels (Miall, 1978, 2000). Deltaic foresets on lacustrine margins (Kostic et al., 2005; Winsemann et al., 2007).
Sands (commonly associated with thin layers of silt or mud). Figs. 6, 7A, 7C, 7D.	Grey, yellow and light brown, very coarse to fine particle sand size; polymictic grains; with or without calcareous cement. Generally tabular, with planar or slightly concave bases, and	**Sm:** structureless or with contorted laminae and flames from underlying silt and clay layers. Microfaults. Figs. 6A, 6D, 6G, 7A, 7C, 7D, 9C.	Deposition from a high-velocity expanding flow (Ashley, 2002). Deposition in shallow braided fluvial systems, frequently as

ACCEPTED MANUSCRIPT

	locally lenticular (channel-like). Internal concave surfaces. Up to 1 m thick.	**St**: trough cross-stratification, sets dm thick. **Sp**: planar cross-stratification, sets dm thick.	channel fills (St<> Gt; Sp<>Gp) (Miall, 1978; Allen, 1982). Scour and fill in high-velocity flow conditions.
		Ss: scour and fills, dm thick. Fig. 6E. **Sh**: horizontal lamination; clay flames and convoluted laminae. Figs. 6A, 6E, 9B, 9C, 9E, 9F. **Sr1**: with ripple lamination and climbing ripples, mostly of type B (with stoss and lee laminae), with mud drapes. Contorted laminae. Figs. 6A to 6D, 9D. **Sr2**: with small scale cross lamination, current ripples. Figs. 5G, 6G. **Sf**: foreset cross-stratification. Sigmoid- and lense-shaped bodies dm thick. Fig. 6F.	Traction from turbidite flows (Allen, 1982; Johnsen and Brennand, 2006). Lacustrine deposition from successive high-velocity expanding sheet flows in prodelta and distal areas (Blair, 1987). Sr, and associated Sh: Traction and suspension from turbitity currents forming ripples and laminae in delta foresets, prodelta and distal lake areas (Mulder and Alexander, 2001; Johnsen and Brennand, 2006 and references therein). Sr1: high deposition rates. Soft sediment deformation Deltaic foresets on lake margins (Arenas et al., 1989; Winsemann et al., 2007), commonly associated with Sf.
Silts. In many cases, alternating with or interbedded within fine sands and/or clays. Figs. 7A, 7B, 7C, 8A, 8B	Yellow to light brown. Tabular deposits up to 2 m thick, consisting of single bodies 1 to 15 cm thick. Common dropstones mm to cm long.	**Fm:** structuress or with fine-sand flames and contorted laminae. Fig. 7C, D, E. **Fr**: climbing ripple lamination (type B) and lenticular stratification. Fig. 7A. **Fh**: horizontal lamination and	Lacustrine deposition in prodelta and distal lake area. Traction current activity (Evans et al., 2013) and, for Fh and Fm, also suspension settling. Iceberg-rafting of dropstones.

ACCEPTED MANUSCRIPT

		layering (silt layers 2-3 cm thick). Figs. 7C, 8A, 8B.	
Clays. In some cases, including mm to sub-mm silt laminae. Figs. 7B to 7F, 8.	Grey, green and ochre. Yellow to beige. Tabular deposits up to 4.5 m thick, commonly consisting of tabular layers 2 to 15 cm thick distinguished by colour. Common dropstones mm to ca. 1 m long.	**Clm**: structureless. At places with folding (slumps). Fig. 7B, D, E, F. **Clh:** horizontal lamination; very thin (mm to sub-mm thick) rythmic laminae that are grouped in layers up to 15 cm thick. At places with folding (slumps). Figs. 7B to 7F, 8A to 8D.	Offshore (distal lake area), uniform (Clm) or rhythmic deposition (Clh), mainly from suspension settling. Iceberg-rafting of dropstones (Ashley, 2002; Johnsen and Brennand, 2006; Evans et al., 2013).

ACCEPTED MANUSCRIPT

ACCEPTED MANUSCRIPT

Table 2. Optically Stimulated Luminiscence (OSL) dates from glacial and glaciolacustrine deposits on the River Sorrosal valley (adapted from Sancho et al., 2011). Location of glaciolacustrine dated samples is shown in figure 3 (LB1 stratigraphic section). Depth refers to thickness downward from the top of section (i.e., outcropping deposit).

Laboratory code	Location	Depth (m)	De (Gy)	Dose rate (mGy/a)	OSL date BP (ka)
X1598	Glaciolacustrine deposit (Section LB1, Unit 2)	22.5	64 ± 14	1.32 ± 0.06	49 ± 11
X1599	Glaciolacustrine record (Section LB1, Unit 2)	29.5	100 ± 5	1.22 ± 0.06	82 ± 6
X1600	Glaciolacustrine record (Section LB1, Unit 2)	35	75 ± 12	1.36 ± 0.06	55 ± 9
X1601	Kame terrace deposits Moraine of Viu	3	86 ± 13	1.75 ± 0.08	49 ± 8

Table 3. Summary of ages obtained in the studied Sorrosal valley and in Pleistocene glacial and fluvial records relevant to this study in the northeastern Iberian Peninsula. Location of points and correspondent authors in Fig. 1B.

PYRENEES AND EBRO BASIN (overall data) (Sites located in Fig. 1B, this work)	**AGE Ka (BP)**	**Marine Isotope Stage (age ka)**	**LINÁS DE BROTO-VIU (this work)** (Figs. 2 and 3, Table 2)	**OSL dates ka (BP)**
		MIS 2		
		29-30		
5-Moraine b, Valira Valley (Andorra)	32	**MIS 3**	Fragen moraine	

ACCEPTED MANUSCRIPT

6-Moraine, Ariège Valley (France)	35			
2a-Moraine, Senegüé (River Gállego)	36±3			
			Units 3, 4 and 5 (LB 1)	
2c-Fluvial terrace aggradation (River Gállego)	45±3		Viu moraine (kame terrace)	49±8
4b-Fluvial terrace aggradation (River Cinca, Qt8)	47±4			49±11
			Unit 2 (LB1)	55±9
			Unit 1 (LB1)	> 55±9
		60-61		
5-Moraine a, Valira Valley (Andorra)	59±1		MAXIMUM EXTENT OF THE ARA GLACIER	
4c-Terrace Qt7 (River Cinca)	61±4			
4a-Terminal moraine, Salinas de Sin (River Cinca/Cinqueta)	64±11			
2b-Glaciofluvial terraces (River Gállego)	68±7	**MIS 4**		
1b-Moraine, Castiello (River Aragón)	68±7			
1a-Fluvial terrace, Aragón valley (River Aragón)				

ACCEPTED MANUSCRIPT

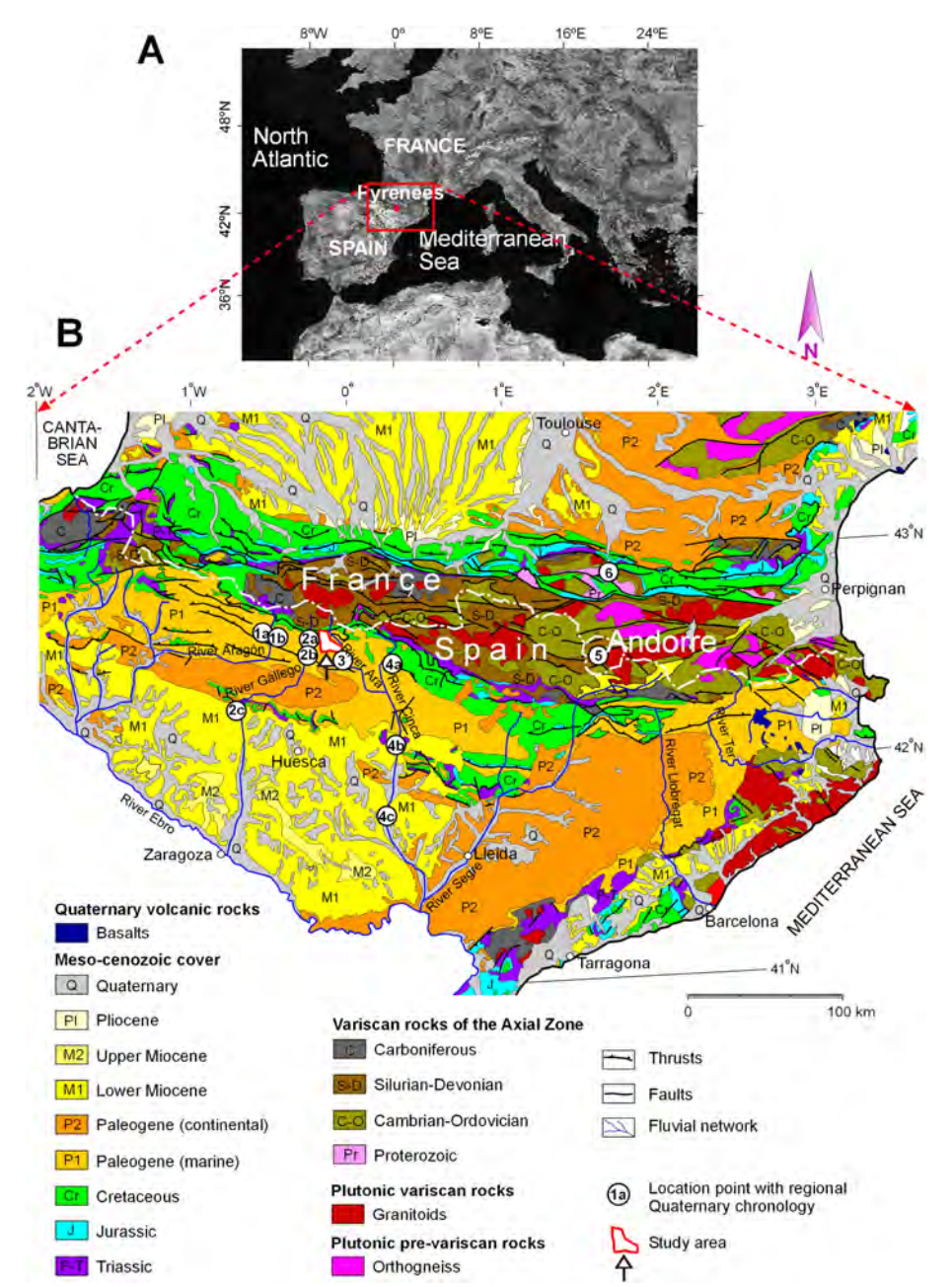
A
8°W
0°
8°E
16°E
24°E
48°N
42°N
36°N
North Atlantic
FRANCE
Pyrenees
SPAIN
Mediterranean Sea
B
N
2°W
1°W
0°
1°E
2°E
3°E
CANTA-BRIAN SEA
Toulouse
France
Spain
Andorra
Perpignan
Huesca
Zaragoza
Lleida
Barcelona
Tarragona
River Aragon
River Gallego
River Cinca
River Ebro
River Segre
River Llobregat
River Ter
MEDITERRANEAN SEA
43°N
42°N
41°N
0
100 km
Quaternary volcanic rocks
Basalts
Meso-cenozoic cover
Q Quaternary
Pl Pliocene
M2 Upper Miocene
M1 Lower Miocene
P2 Paleogene (continental)
P1 Paleogene (marine)
Cr Cretaceous
J Jurassic
T-Tr Triassic
Variscan rocks of the Axial Zone
C Carboniferous
S-D Silurian-Devonian
C-O Cambrian-Ordovician
Pr Proterozoic
Plutonic variscan rocks
Granitoids
Plutonic pre-variscan rocks
Orthogneiss
Thrusts
Faults
Fluvial network
1a Location point with regional Quaternary chronology
Study area

Figure 1

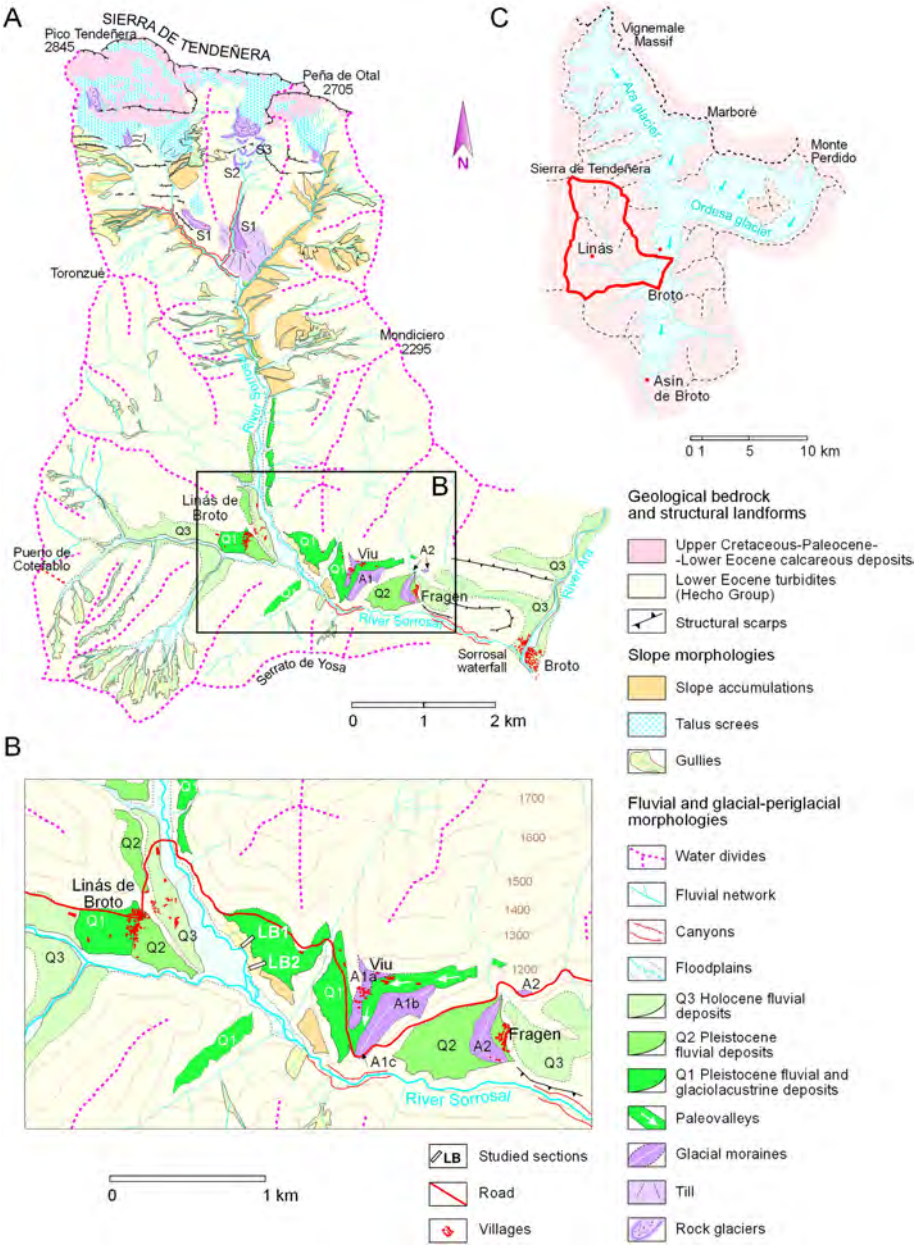
A
SIERRA DE TENDEÑERA
Pico Tendeñera
2845
Peña de Otal
2705
S3
S2
S1
S1
Toronzue
Mondiciero
2295
River Sorrosal
B
Linás de
Broto
Q3
Q1
Q1
Viu
A2
A1
Q2
Fragen
Q3
Q3
River Ara
River Sorrosal
Puerto de
Cotefablo
Serrato de Yosa
Sorrosal
waterfall
Broto
0
1
2 km
N
C
Vignemale
Massif
Ara glacier
Marboré
Monte
Perdido
Sierra de Tendeñera
Ordesa glacier
Linás
Broto
Asin
de Broto
0 1
5
10 km
B
Q2
Linás de
Broto
Q1
Q3
Q2
Q3
LB1
LB2
Viu
A1a
Q1
A1b
A2
Q1
Q2
A2
Fragen
A1c
Q3
River Sorrosal
1700
1600
1500
1400
1300
1200
0
1 km
LB
Studied sections
Road
Villages
Geological bedrock
and structural landforms
Upper Cretaceous-Paleocene-
-Lower Eocene calcareous deposits
Lower Eocene turbidites
(Hecho Group)
Structural scarps
Slope morphologies
Slope accumulations
Talus screes
Gullies
Fluvial and glacial-periglacial
morphologies
Water divides
Fluvial network
Canyons
Floodplains
Q3 Holocene fluvial
deposits
Q2 Pleistocene
fluvial deposits
Q1 Pleistocene fluvial and
glaciolacustrine deposits
Paleovalleys
Glacial moraines
Till
Rock glaciers

Figure 2

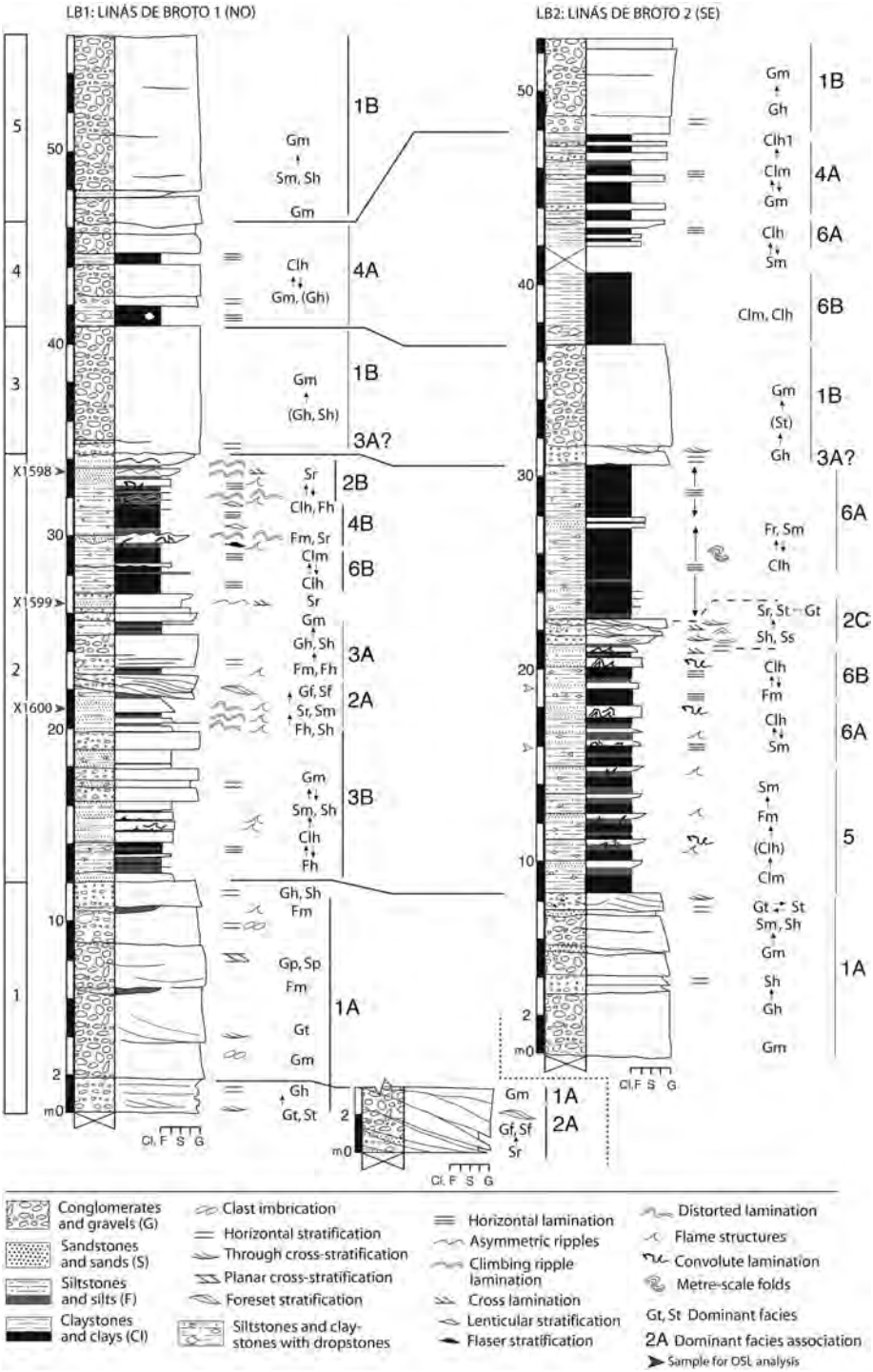
LB1: LINÁS DE BROTO 1 (NO)
LB2: LINÁS DE BROTO 2 (SE)
X1598
X1599
X1600
Cl, F S G
Conglomerates and gravels (G)
Sandstones and sands (S)
Siltstones and silts (F)
Claystones and clays (Cl)
Siltstones and claystones with dropstones
Clast imbrication
Horizontal stratification
Through cross-stratification
Planar cross-stratification
Foreset stratification
Horizontal lamination
Asymmetric ripples
Climbing ripple lamination
Cross lamination
Lenticular stratification
Flaser stratification
Distorted lamination
Flame structures
Convolute lamination
Metre-scale folds
Gt, St Dominant facies
2A Dominant facies association
Sample for OSL analysis

Figure 3

Figure 4

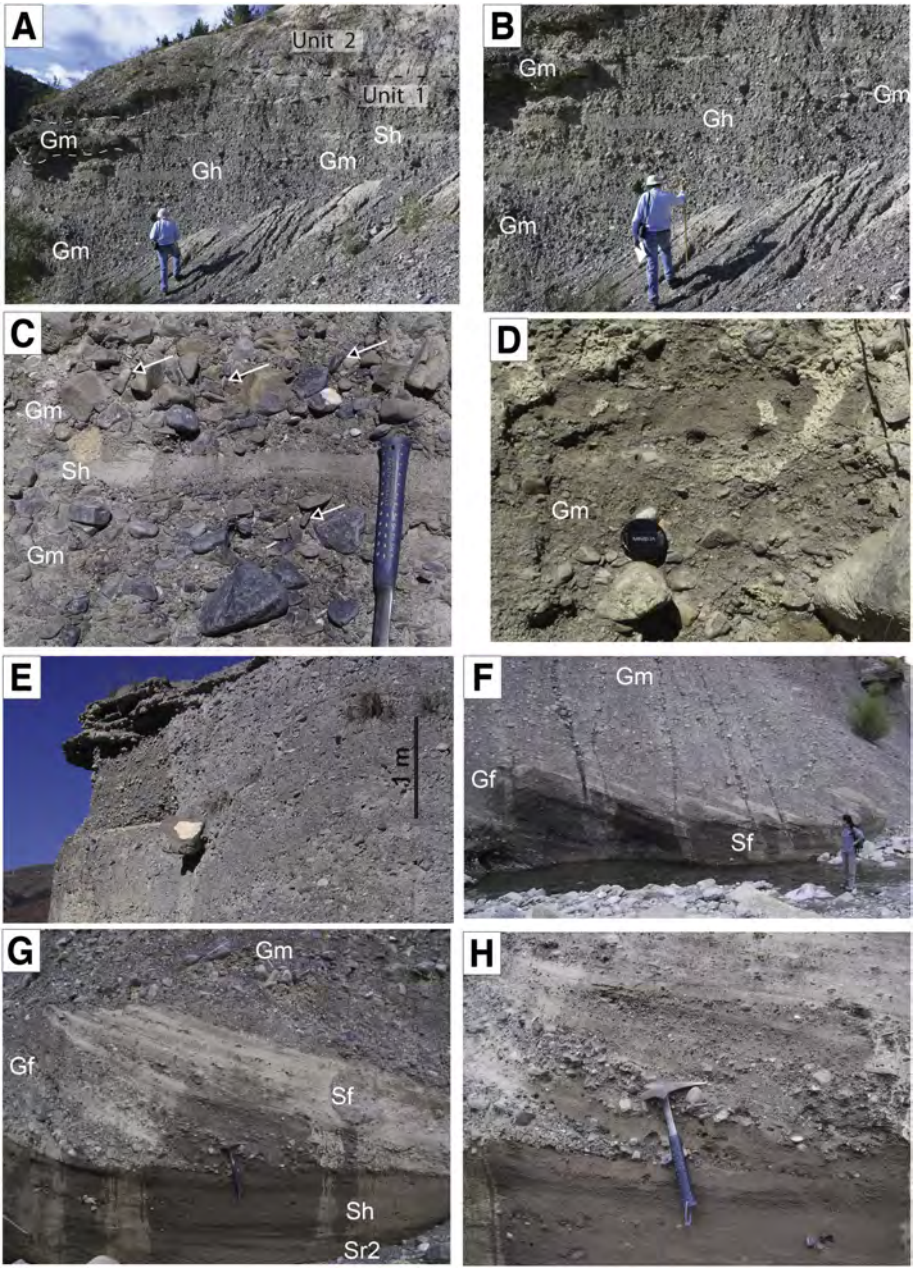
A
Unit 2
Unit 1
Gm
Gh
Gm
Sh
Gm
B
Gm
Gh
Gm
Gm
C
Gm
Sh
Gm
D
Gm
E
1 m
F
Gm
Gf
Sf
G
Gm
Gf
Sf
Sh
Sr2
H

Figure 5

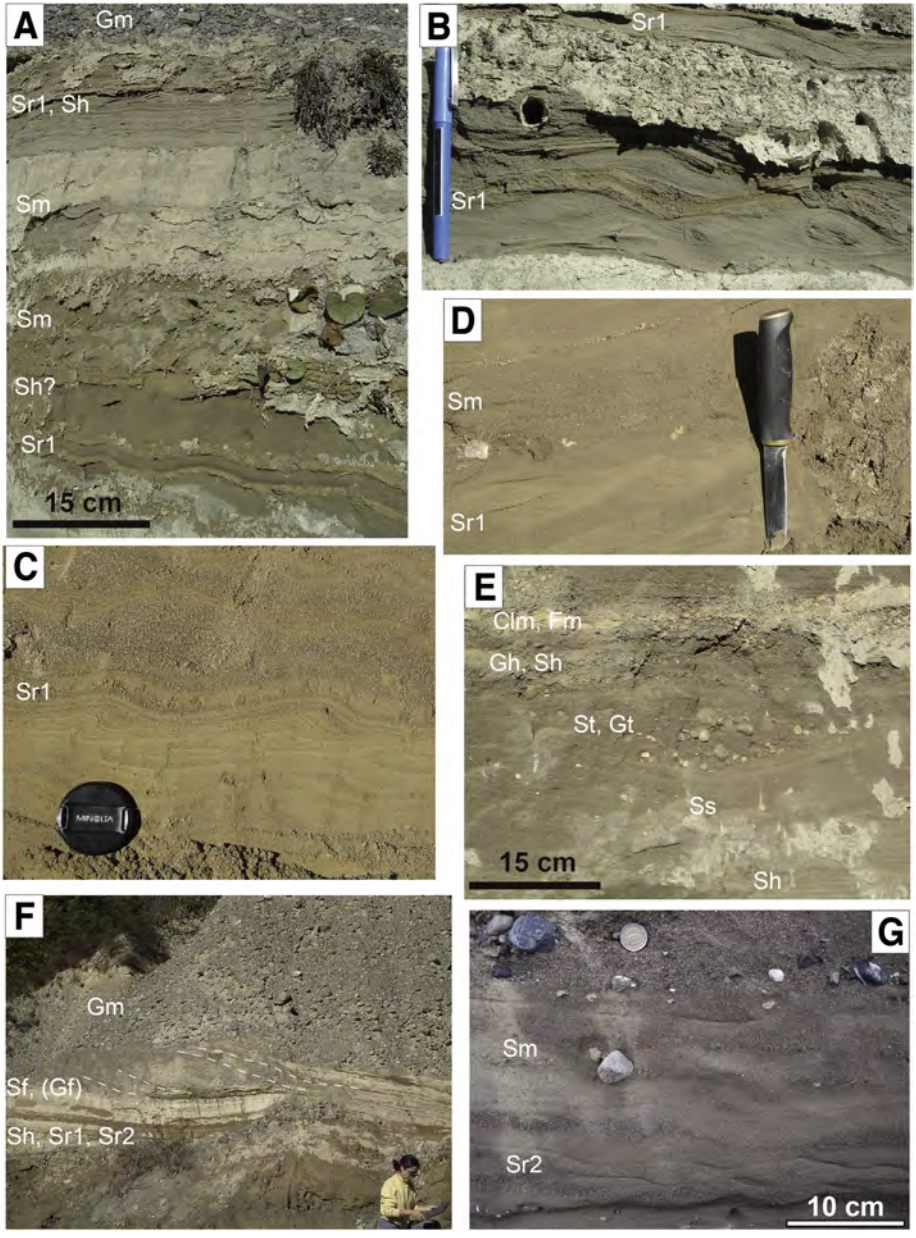
A
Gm
Sr1, Sh
Sm
Sm
Sh?
Sr1
15 cm
B
Sr1
Sr1
D
Sm
Sr1
C
Sr1
E
Clm, Fm
Gh, Sh
St, Gt
Ss
15 cm
Sh
F
Gm
Sf, (Gf)
Sh, Sr1, Sr2
G
Sm
Sr2
10 cm

Figure 6

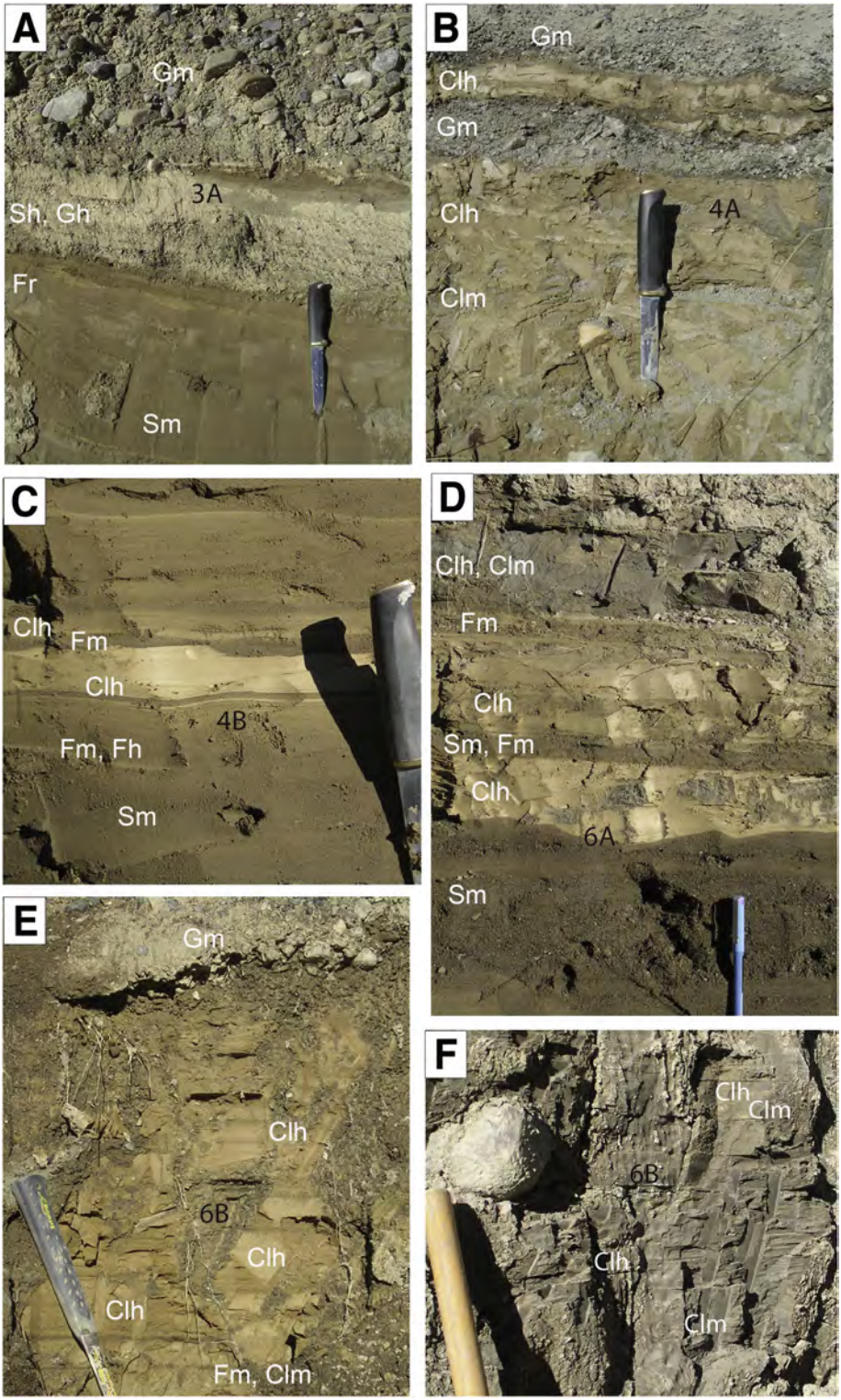
A
Gm
3A
Sh, Gh
Fr
Sm
B
Gm
Clh
Gm
Clh
4A
Clm
C
Clh
Fm
Clh
4B
Fm, Fh
Sm
D
Clh, Clm
Fm
Clh
Sm, Fm
Clh
6A
Sm
E
Gm
Clh
6B
Clh
Clh
Fm, Clm
F
Clh
Clm
6B
Clh
Clm

Figure 7

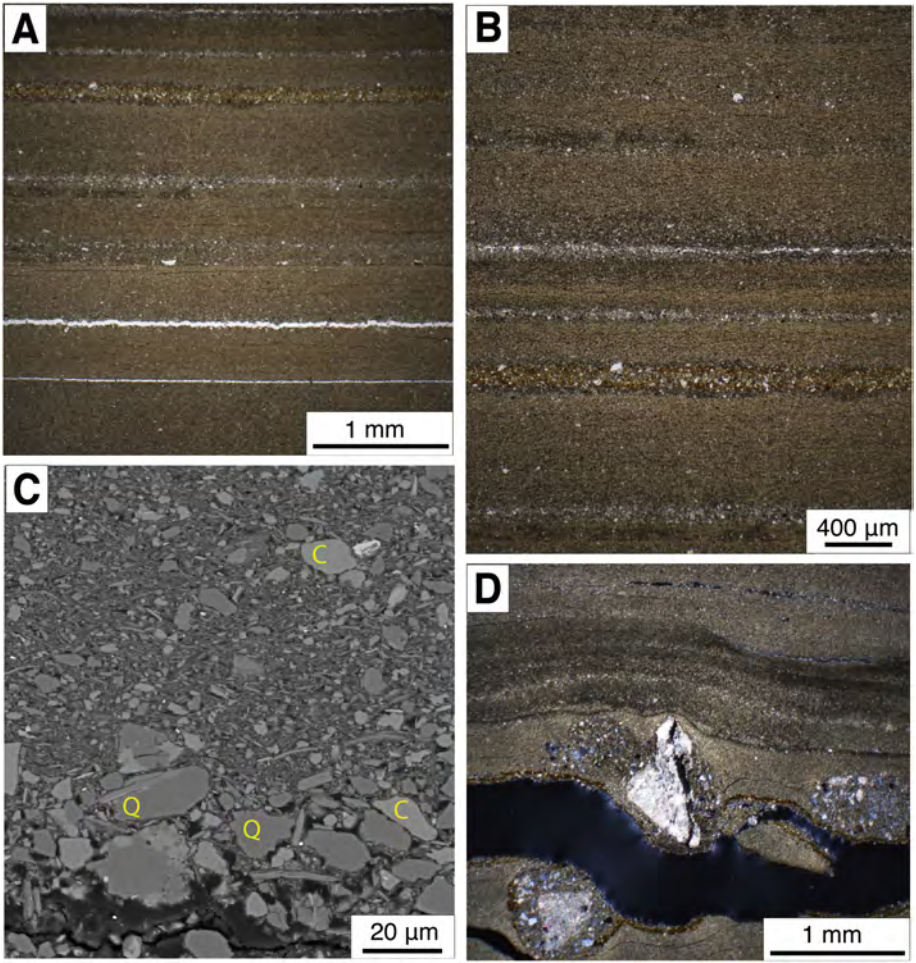

Figure 8

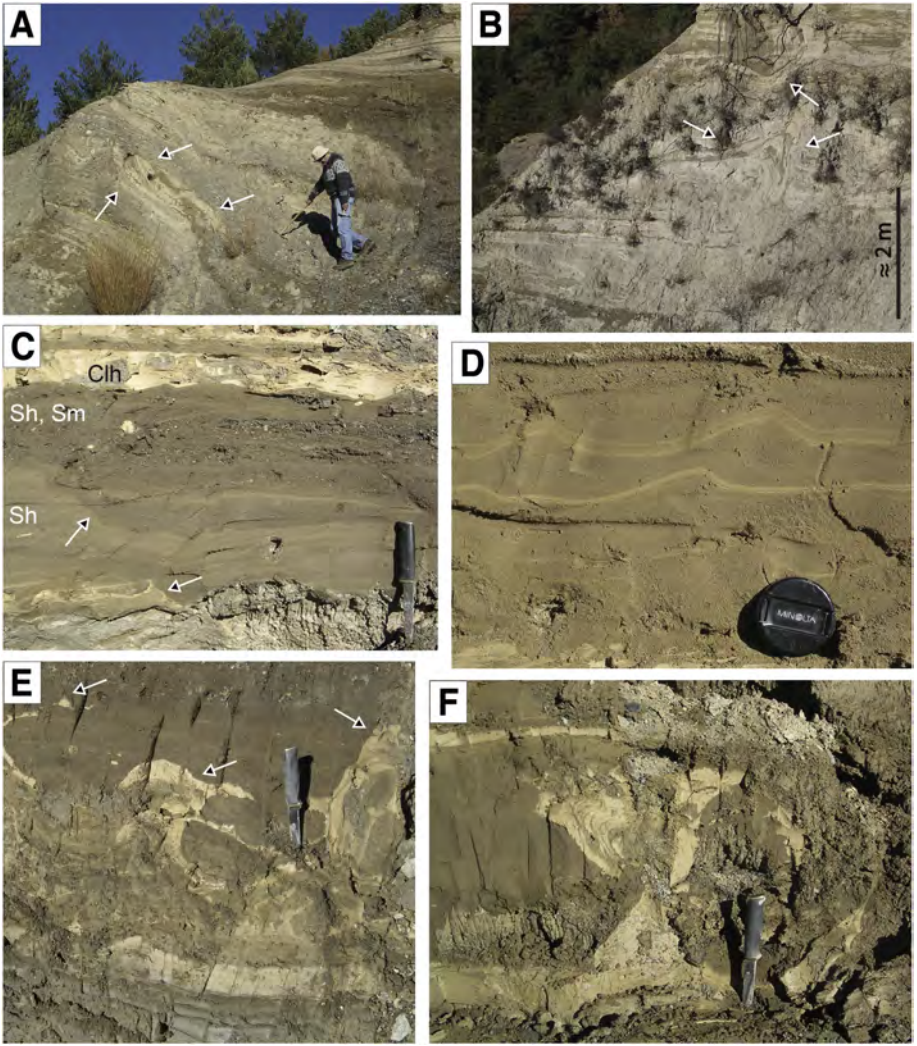

Figure 9

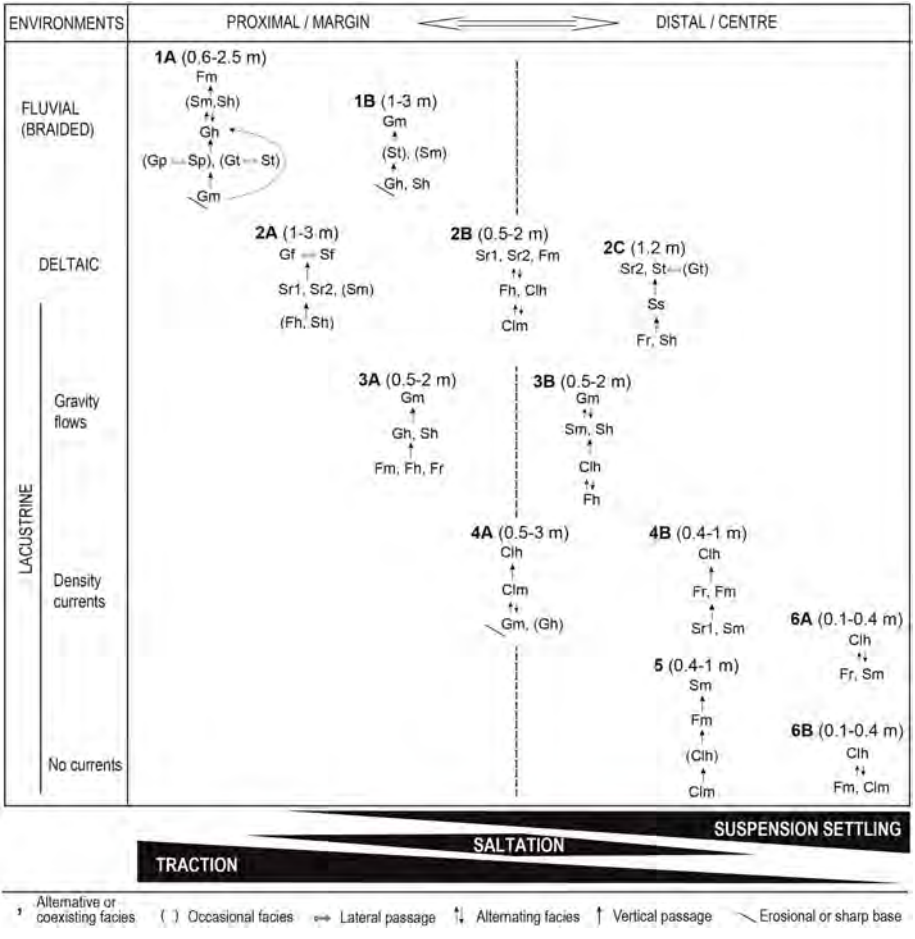
ENVIRONMENTS
PROXIMAL / MARGIN
DISTAL / CENTRE
FLUVIAL (BRAIDED)
DELTAIC
LACUSTRINE
Gravity flows
Density currents
No currents
1A (0.6-2.5 m)
Fm
(Sm,Sh)
Gh
(Gp Sp), (Gt St)
Gm
1B (1-3 m)
Gm
(St), (Sm)
Gh, Sh
2A (1-3 m)
Gf Sf
Sr1, Sr2, (Sm)
(Fh, Sh)
2B (0.5-2 m)
Sr1, Sr2, Fm
Fh, Clh
Clm
2C (1.2 m)
Sr2, St (Gt)
Ss
Fr, Sh
3A (0.5-2 m)
Gm
Gh, Sh
Fm, Fh, Fr
3B (0.5-2 m)
Gm
Sm, Sh
Clh
Fh
4A (0.5-3 m)
Clh
Clm
Gm, (Gh)
4B (0.4-1 m)
Clh
Fr, Fm
Sr1, Sm
5 (0.4-1 m)
Sm
Fm
(Clh)
Clm
6A (0.1-0.4 m)
Clh
Fr, Sm
6B (0.1-0.4 m)
Clh
Fm, Clm
SUSPENSION SETTLING
SALTATION
TRACTION
Alternative or coexisting facies
( ) Occasional facies
Lateral passage
Alternating facies
Vertical passage
Erosional or sharp base

Figure 10

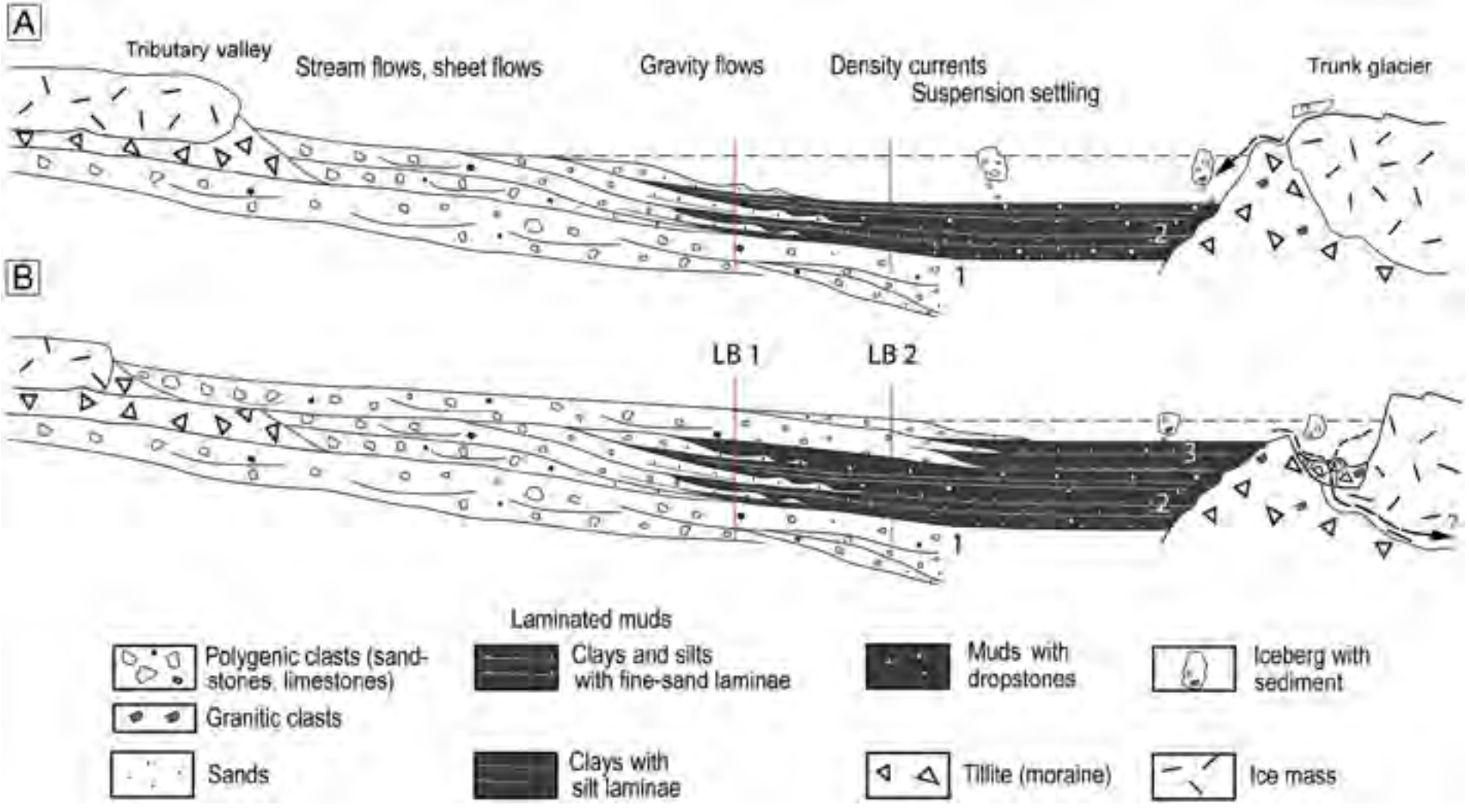
A
Tributary valley
Stream flows, sheet flows
Gravity flows
Density currents
Suspension settling
Trunk glacier
1
2
B
LB 1
LB 2
1
2
3
Laminated muds
Polygenic clasts (sand-stones, limestones)
Granitic clasts
Sands
Clays and silts with fine-sand laminae
Clays with silt laminae
Muds with dropstones
Tillite (moraine)
Iceberg with sediment
Ice mass

Figure 11

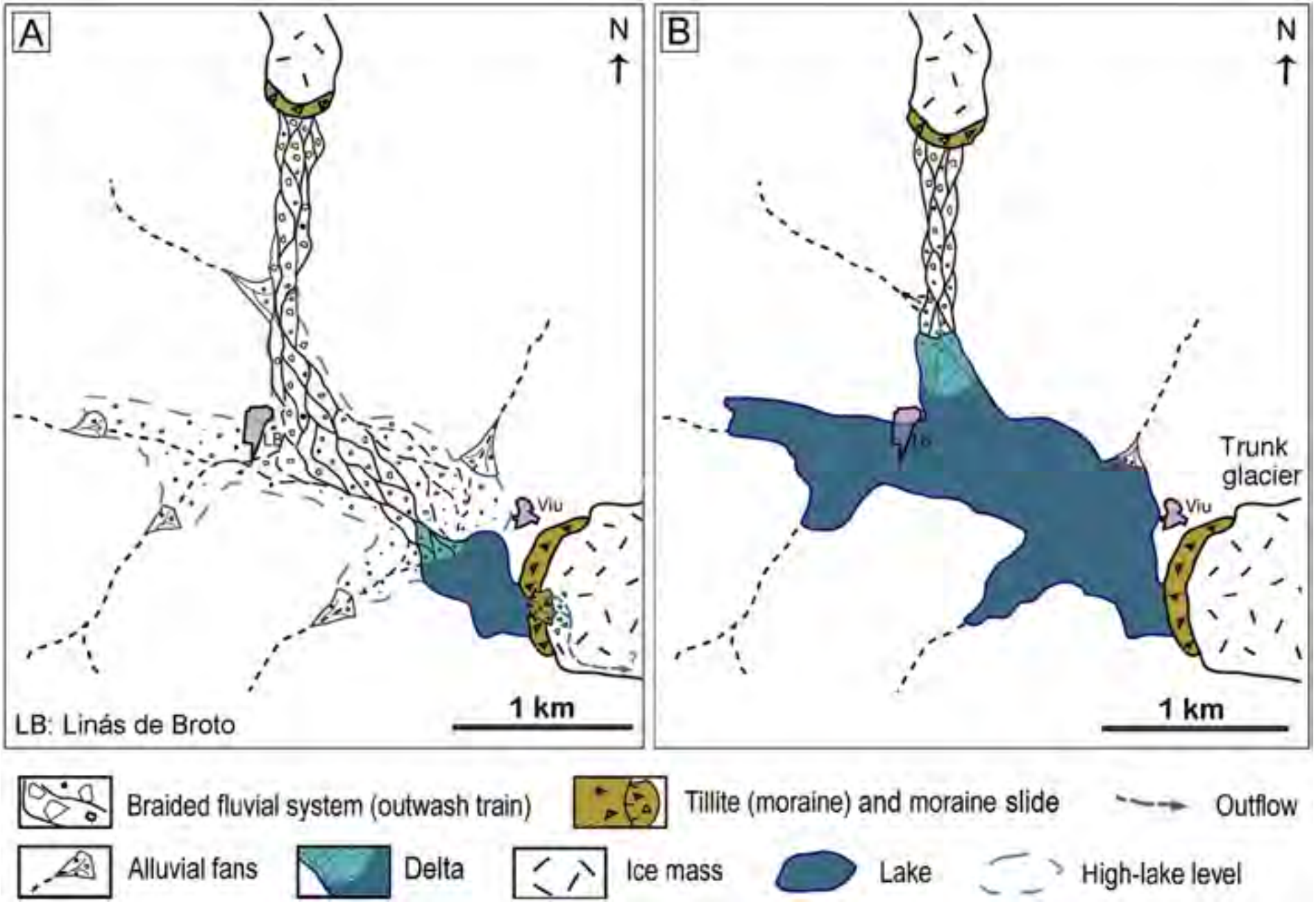
A
N
LB
Viu
1 km
LB: Linás de Broto
B
N
Trunk glacier
Viu
1 km
Braided fluvial system (outwash train)
Tillite (moraine) and moraine slide
Outflow
Alluvial fans
Delta
Ice mass
Lake
High-lake level

Figure 12